Nano Research

Open Access

Review Article

Dynamic processes of oxygen reduction reaction: Insights from theoretical simulations and *in-situ* characterization

Linkai Han[1] ✉, Jiemeng Luo[1], Yu Sun[1], Huidi Yu[2], Yiheng Li[2], Xiaodan Liu[2], Xiaoqi Wang[2] ✉, and Jianming Li[1] ✉

[1] *School of New Energy, Ningbo University of Technology, Ningbo 315211, China*
[2] *Research Institute of Petroleum Exploration & Development, PetroChina, Beijing 100083, China*

Cite this article: *Nano Research*, **2026**, *19*, 94908550. https://doi.org/10.26599/NR.2026.94908550

ABSTRACT: Oxygen reduction reaction (ORR) is critical cathodic process in energy conversion devices such as proton exchange membrane fuel cells (PEMFCs). Its sluggish kinetics severely limit the efficiency and commercialization prospects. However, catalysts design strategies based on the static initial structures often fail to adequately capture the genuine working state and reaction mechanisms under realistic electrochemical conditions. Here we systematically outline recent significant progress in elucidating the ORR process through dynamic theoretical simulations and *in-situ* characterization. The role of dynamic simulations (electrolyte environment, applied potential, pH dependence, and ions effects) in understanding the evolution of catalyst structures and reaction processes under practical conditions was discussed. Meanwhile, the applications of *in-situ* X-ray absorption spectroscopy (XAS), vibrational spectroscopy (Raman spectroscopy, Fourier transform infrared spectroscopy), and microscopic in the evolution of catalyst electronic states and the behavior of reaction intermediates during the ORR process were summarized. Through the mutual validation of theory and experiment, we clarify the decisive regulatory role of the dynamic interfacial microenvironment on activity. Finally, based on dynamic research, the rational design principles and future research directions of electrocatalysts for actual reaction conditions were prospected.

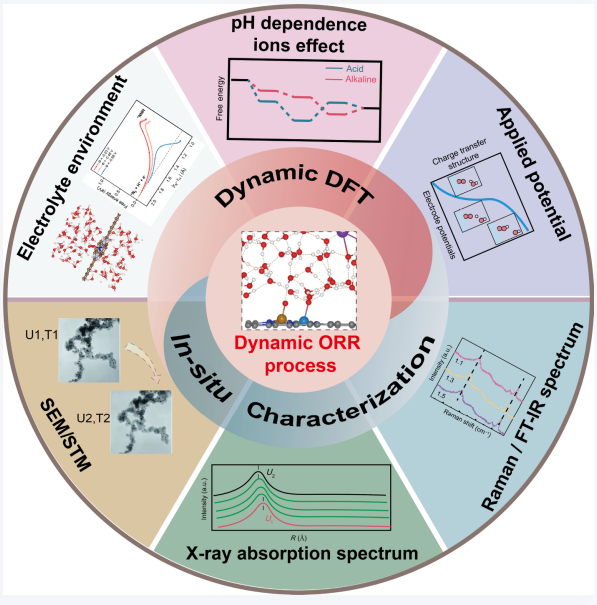

KEYWORDS: oxygen reduction reaction, dynamic interfaces, theoretical simulations, *in-situ* characterization, electrochemical environments, M-N-C catalyst

1 Introduction

The accelerated global transition towards a low-carbon energy structure has positioned the development of efficient and cost-effective energy storage and conversion technologies as a central challenge in addressing energy crises and environmental issues [1, 2]. The oxygen reduction reaction (ORR), being the pivotal cathodic reaction in next-generation energy conversion devices like proton exchange membrane fuel cells (PEMFCs) and metal-air batteries, relies heavily on high-efficiency catalysts to overcome its substantial kinetic barriers [3, 4]. Consequently, catalyst performance directly determines the energy conversion efficiency and operational lifespan of these devices [5, 6]. Platinum (Pt)-based noble metal catalysts have long been the benchmark due to their high activity. However, their high cost, limited natural abundance, and insufficient long-term stability severely hinder large-scale commercial adoption [7–10]. Thus, developing low-cost, high-performance non-precious metal ORR catalysts has become a central focus and a significant challenge in energy catalysis.

Among numerous candidate materials, atomically dispersed metal-nitrogen-carbon (M-N-C) catalysts have shown immense potential as alternatives to noble metals [11–13]. Traditional research has established preliminary structure–activity by tuning initial physicochemical properties, such as metal center type,

Received: December 24, 2025; **Revised:** January 28, 2026
Accepted: February 8, 2026

✉Address correspondence to Linkai Han, hanlkag@163.com; Xiaoqi Wang, wangxq07@petrochina.com.cn; Jianming Li, jmli@nbut.edu.cn

coordination environment, and carbon support structure, from a static perspective [14–19]. However, the realistic electrochemical environment is inherently dynamic [27–30]. Factors including electrolyte solvation [25, 31–33], electron transfer under applied potential [25, 30, 34, 35], and proton-coupled effects induced by pH variations [29, 36–39] will lead to continuous changes in the structure, electronic state, and interface interactions of the catalyst active site. This dynamic interaction often leads to significant differences between the actual working state of the catalyst and its initial static structure (Fig. 1) [27]. Conventional static research methods are inadequate for fully unveiling the intrinsic mechanisms of ORR catalysis, thereby impeding the precise design of catalysts.

Recent breakthroughs in theoretical simulations and characterization techniques have provided crucial tools for analyzing catalyst dynamics [40–42]. The introduction of dynamic density functional theory (DFT) calculations beyond traditional vacuum conditions has accelerated the understanding of the performance regulation mechanisms of active sites by factors such as solvents, potential, and ions in electrochemical environments [43–46]. These approaches have revealed novel phenomena, including potential-dependent shifts in the rate-determining step (RDS) [47–50]. Experimentally, the rapid development of *in-situ* characterization techniques allows real-time observation during ORR: *In-situ* X-ray absorption spectroscopy (XAS) tracks changes in metal oxidation states and coordination environments [51–53]; *in-situ* Raman and *in-situ* Fourier transform infrared spectroscopy (*in-situ* FTIR) identify the adsorption and conversion of reaction intermediates [54–56]; and *in-situ* microscopy visualizes morphological changes and aggregation behavior of active sites [26, 57, 58].

Combining *in-situ* characterization and theoretical simulations [59–62] has overcome the limitations of static studies, establishing crucial links between dynamic structure, environmental modulation, and catalytic performance, thereby offering a new dimension for catalyst optimization (Fig. 2).

Here we reviewed recent progress in dynamic studies of ORR, focusing on understanding how the dynamic interplay between catalysts and the electrochemical environment influences and regulates ORR performance. We first briefly revisit the development and screening of M-N-C catalysts, along with the fundamentals of static structural simulations. Subsequently, we emphasize the latest advances in dynamic theoretical simulation methods for electrochemical interfaces (electrolyte environment, applied potential, pH dependence, and ions effects) and *in-situ* characterization. Furthermore, we summarized cases in ORR and other electrocatalytic fields where the regulatory mechanisms of electrocatalytic activity were jointly revealed by combining dynamic DFT and *in-situ* characterization. Finally, we summarize catalyst design strategies tailored for realistic reaction conditions and outline future research directions. This review provides a reference for the design of high-performance electrocatalysts (extending beyond ORR), fostering a paradigm shift from static structure-based to dynamic environment-aware catalyst design, and accelerating their practical application in energy conversion devices.

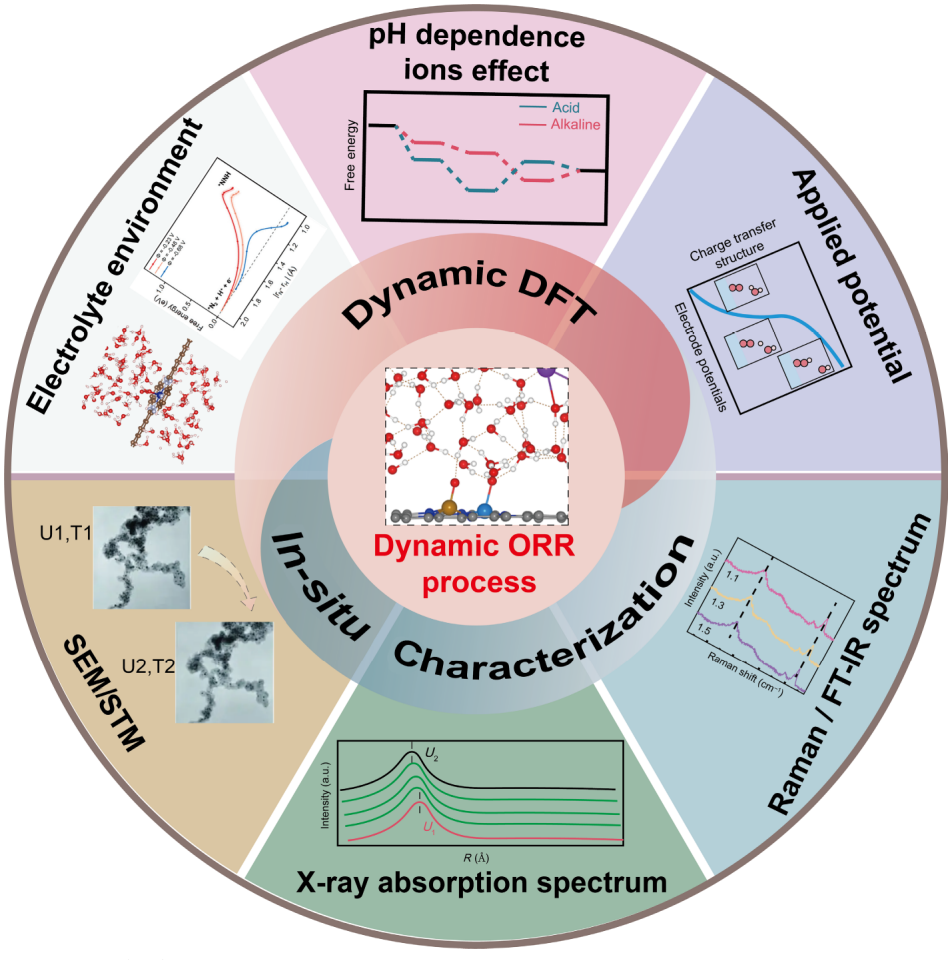

Figure 1 Overview of the topics covered in this review.

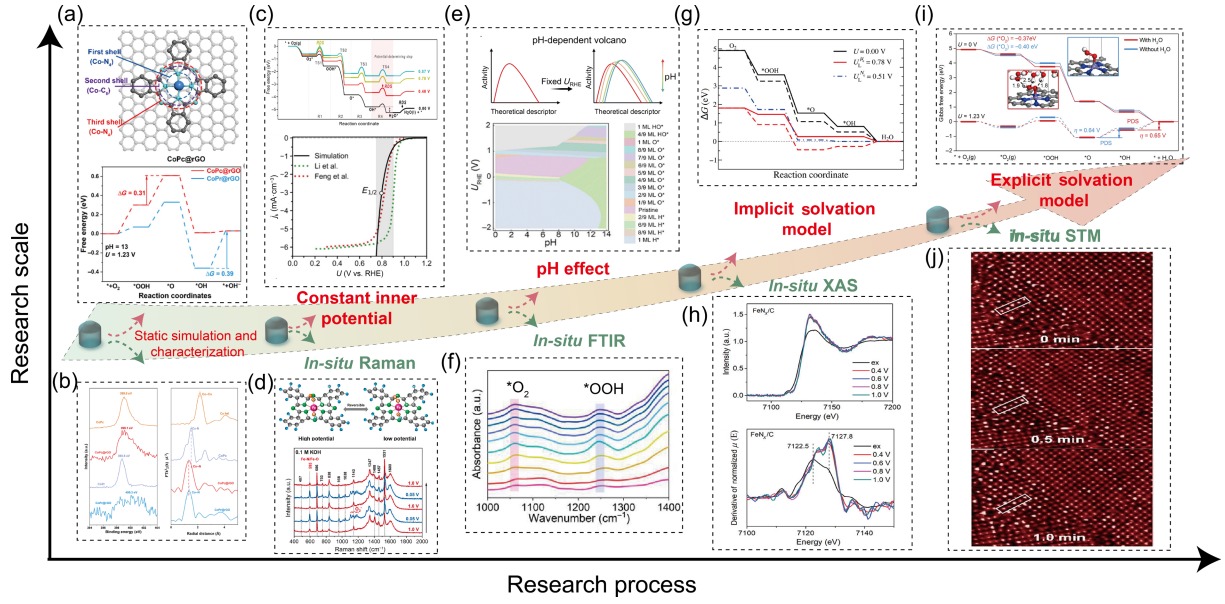

Figure 2 ORR ranges from static studies to multi-method dynamic process studies. (a) Static ORR process simulation at the MN_4 site. (b) Static structural characterization of M-N-C catalysts. Reproduced with permission from Ref. [18], © American Chemical Society 2025. (c) DFT simulation of the ORR process under constant potential correction and the corresponding electrochemical performance fitting. Reproduced with permission from Ref. [30], © American Chemical Society 2025. (d) *In-situ* Raman characterization of M-N-C catalysts. Reproduced with permission from Ref. [20], © American Chemical Society 2022. (e) The influence of pH effect on the adsorption energy of multiple reactive adsorption species. Reproduced with permission from Ref. [21], © Liu, H. et al. 2024. (f) *In-situ* infrared characterization of the ORR process and identification of key reaction intermediates. Reproduced with permission from Ref. [22], © American Chemical Society 2025. (g) The influence of implicit solvation models on the free energy of the ORR process. Reproduced with permission from Ref. [23], © American Chemical Society 2023. (h) *In-situ* XAS characterization of the ORR process. Reproduced with permission from Ref. [24], © American Chemical Society 2019. (i) The influence of explicit solvation models on the free energy of the ORR process. Reproduced with permission from Ref. [25], © American Chemical Society 2023. (j) STM characterization of ORR catalysts. Reproduced with permission from Ref. [26], © Wiley-VCH 2016.

2 Overview of M-N-C materials for ORR and basis for static simulation

With the proposal of single-atom catalysts, M-N-C catalysts have achieved rapid development and breakthroughs in the field of ORR [66, 67]. Before delving into the dynamic effects of the reaction environment on the M-N-C catalyst, it is crucial to first review its classic static structural model and the latest research advancements. These studies based on static environments can further deepen our understanding of dynamic ORR research.

After the M-N-C material was first applied in ORR [68, 69], researchers conducted numerous experiments and theoretical studies on different types of M-N-C materials. Up to now, the FeN_4 active site is regarded as the most promising active structure [70, 71]. Although the stability issue of Fe-N-C materials under acidic ORR cannot be further applied to long-running energy conversion devices such as PEMFCs [72, 73], researchers can effectively improve the stability and activity by optimizing their geometric or electronic structures through various strategies [18, 63–65, 74–76]. For example, the latest research [63] demonstrates that FeN_4 sites fabricated on the inner concave curved surface of nano springs deliver enhanced activity from the graphitized outer carbon layer, while the outer carbon layer also shields the active sites to improve stability (Fig. 3(a)). This material can still maintain 86% activity after operating for more than 300 h at a hydrogen-air pressure of 1.0 bar. This study also conducted *in-situ* XAS tests on the synthesized materials under the working voltage of ORR, but the X-ray absorption near edge structure (XANES) and extended X-ray absorption fine structure (EXAFS) data of Fe atoms is the average value of all Fe atom structures in the material, which is also the most significant limitation of *in-situ* XAS testing in the research of M-N-C catalysts [52, 77]. The high-temperature carbonization brings uncertain carbon defects while the constructed active centers are not always FeN_4 [28, 78–80], which still poses a challenge to improving the ORR stability of Fe-N-C. Therefore, by analyzing the stability decay mechanism of FeN_4 sites in the ORR through dynamic DFT simulation and combining with *in-situ* evidence, new stable M-N-C type ORR catalysts can be further efficiently developed.

In addition to the construction of single-atom FeN_4 sites, many researchers have also proposed various interesting and efficient strategies such as dual atom catalysts (DACs) [64, 74, 81–85], FeN_5 sites [76, 86–88], and doping with heteroatoms [65, 85, 89–91] to optimize catalytic activity. Although these strategies have great potential in improving activity and stability, they also reveal more issues that require the combination of dynamic DFT simulations and *in-situ* characterization techniques to resolve. For instance, Yu et al. [64] achieved a simultaneous enhancement of activity and stability by constructing a Fe-Ru dual-atom active site (Fig. 3(b)). Ru atoms were introduced near the Fe site as an electron buffering site. After a long-term stability test, the retention rate of iron exceeded 97%, significantly reducing the dissolution of active Fe. Although this work demonstrated that the construction of bimolecular active sites can enhance catalytic activity, the high-temperature carbonization process can form multiple configurations of bimolecular sites [92]. Different configurations often cannot be evaluated for their activity using the same static calculation method. Our previous research [27] has shown that the current $M_1M_2N_6$ configuration formed by the dual-atom M-N-C catalysts not only includes two MN_4 sites, but may also include two

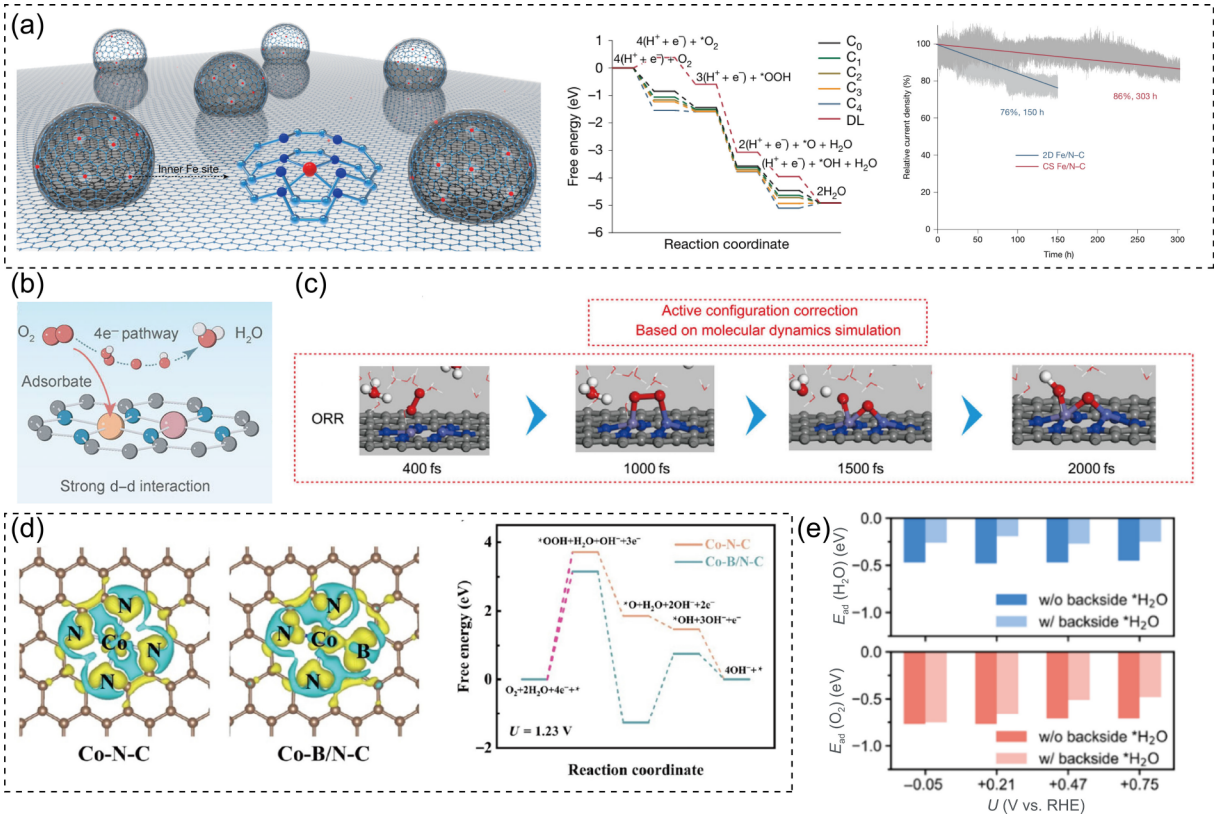

Figure 3 The development and application of M-N-C materials in ORR. (a) The structure of the CS Fe/N-C catalyst, the corresponding intrinsic activity free energy diagram based on static calculations, and its stability in PEMFCs. Reproduced with permission from Ref. [63], © Zhao, Y. S. et al. 2025. (b) The mechanism for enhancing the stability of the Fe-Ru DACs configuration. Reproduced with permission from Ref. [64], © Wiley-VCH GmbH 2025. (c) The dynamic structural evolution of the $M_1M_2N_6$ configuration with two MN_3 sites in the ORR. Reproduced with permission from Ref. [27], © American Institute of Chemical Engineers 2024. (d) The structural model and charge density diagram of the B-doped Co-N-C structure, as well as the corresponding static calculation free energy diagram. Reproduced with permission from Ref. [65], © Qi, Y. G. et al. 2025. (e) Comparison of adsorption energies of oxygen-containing species when solvents are present on the surface. Reproduced with permission from Ref. [30], © American Chemical Society 2025.

MN_3 sites. For the latter case, there is a significant discrepancy between the theoretical activity obtained through the static environment simulation method and the experimental activity. Subsequently, the solvation model and the constant potential DFT study indicated that the two MN_3 sites were not stable under the reaction potential and would form a more stable M_1-O-M_2 configuration (Fig. 3(c)). The theoretical activity obtained based on the new configuration shows a good correlation with the experimental activity. This further indicates that the ORR studies based on dynamic DFT can deeply reveal the dynamic structural evolution of M-N-C materials during the ORR process, opening up new perspectives for the kinetic research of ORR.

In addition, there are many studies where researchers have investigated the impact on activity by altering the coordinating atoms (such as P, O, S, B) in the first coordination layer. For instance, the catalyst synthesized by Qi et al. [65], which has the active site of CoN_3B_1, achieved a significant enhancement in ORR activity under alkaline conditions. The asymmetric electronic structure can optimize the adsorption strength of the oxygen intermediates, thereby improving the thermodynamic reaction barrier (Fig. 3(d)). However, for the initial MN_4 site, the doping of non-metallic elements may cause some MN_3X_1 sites to break the bonds between metals and non-metallic elements during the reaction process [90]. This is more likely to occur for non-metallic elements with smaller atomic radii. This issue needs to be analyzed through the combined use of dynamic DFT simulation and *in-situ* characterization. In addition, we recently published work [76] showing that ORR activity and stability can also be enhanced by constructing FeN_5 sites with axially coordinated N atoms. However, during the basic static DFT calculation process, we realized that the axial coordinating atoms exposed to the reaction environment of the solvent and electric field might be attacked by water molecules or protons in the solvent, forming more complex coordination configurations. This further strengthened our understanding of the dynamic reaction process of ORR.

As we mentioned above, there are numerous studies on M-N-C materials in the field of ORR. Although some researchers have gradually realized the role of *in-situ* techniques in revealing the reaction mechanism and the structural evolution of active sites in ORR, the existing *in-situ* characterization techniques still have limitations in accurately revealing the dynamic reaction process. Moreover, most studies still use static simulation methods to explain the intrinsic active sources of the materials, which inevitably leads to a significant gap between the experimental conclusions and the theoretical explanations. Over the past decade, researchers have rapidly and profoundly advanced the progress of M-N-C materials in the field of ORR under the guidance of static simulation methods. For example, based on the computational hydrogen electrode (CHE) model and volcano relationship theory proposed by Professor Nørskov [66], the understanding of the excellent ORR activity of FeN_4 was accelerated, and many potential electrocatalysts were screened and developed based on the active descriptors

proposed by Xu et al. [93]. However, the volcano plot curve is drawn based on thermodynamic descriptors, and it reflects the theoretical optimal value of catalytic activity under the assumption that all steps are in equilibrium and there are no kinetic barriers. The performance of actual catalysts is also strongly dependent on kinetic factors. Recent studies have demonstrated through dynamic DFT that the adsorption energy data under the reaction potential differs from that obtained through static calculations (Fig. 3(e)) [30]. This indicates that materials obtained through screening based on traditional static DFT simulations and using thermodynamic data such as adsorption energy and reaction free energy changes may not be able to meet industrial requirements in real reaction environments. In particular, the current development of ORR catalysts based on M-N-C is limited by the insufficient stability under industrial conditions, which urgently requires researchers to deepen their understanding of the dynamic reaction process of ORR and the influencing factors of activity in the real environment.

3 The dynamic electrochemical interface: Theory and simulations

The electrochemical interface is the core site where electrocatalytic reactions occur, and its dynamic evolution behavior exerts a profound influence on both the thermodynamic trends and kinetic processes of reactions. However, most traditional theoretical models are calculated under vacuum conditions and usually ignore key practical factors such as the electrolyte environment, applied potential, pH value, and ionic effects, which leads to significant deviations between theoretical predictions and actual electrochemical systems [29, 47, 48, 94, 95]. With the continuous innovation of computational methods, especially the in-depth integration of DFT with implicit/explicit solvation models, constant-potential calculation frameworks, and double-layer theory, researchers have been able to accurately reveal the dynamic characteristics of electrochemical interfaces at the atomic scale [37, 49, 96, 97]. This chapter systematically reviews the latest research progress in theoretical simulations of electrochemical interfaces, focusing on the modeling methods of electrolyte environments, the application scenarios of constant-potential DFT frameworks, and the microscopic mechanisms of pH and ion effects, aiming to provide a solid theoretical basis for the rational design of high-efficiency electrocatalysts [23, 33, 42, 50].

3.1 Electrolyte environment on ORR

In the process of electrocatalytic reactions, the electrolyte environment plays a decisive role in regulating the stability of reaction intermediates and the selection of reaction paths. Early DFT calculations mostly adopted vacuum models; although such models can provide researchers with preliminary insights into the intrinsic activity of catalyst surfaces, they cannot accurately characterize the real reaction environment of the solid–liquid interface. This over-simplified processing method severely restricts the reliability of theoretical predictions, a problem that is particularly prominent in reactions involving polar molecule adsorption and proton-coupled electron transfer. The development of implicit solvation models has provided a preliminary solution to address this challenge. Such models treat the solvent as a continuous dielectric environment and can effectively simulate solvation effects at a relatively low computational cost. The proposal of implicit solvation models has achieved efficient and accurate predictions of experimental values under low computational costs [40]. The theoretical solvation energy obtained based on the model developed by Andreassi et al. [98] has an average absolute error of only 1.3 kcal·mol^{-1} compared to the experimental values. The excellent computational efficiency enables the consideration of the impact of solvation effects in high-throughput catalyst screening processes.

However, implicit models have inherent limitations, they cannot capture directional interactions such as hydrogen bonds and coordination interactions, which are precisely the key factors determining the stability of reaction intermediates. In contrast, explicit solvation models directly simulate molecular-level interactions at the interface by introducing water molecules or ion clusters, thereby providing a more realistic interface description. For the dynamic process of ORR, the adsorption of the three reaction intermediates (OOH, O, OH) is particularly important for analyzing the thermodynamic intrinsic activity and stability. However, the implicit solvation model alone is insufficient to clearly reveal the differences in the adsorption evolution process of the three adsorption groups in the solvent. And the adsorption ability is greatly influenced by the number of water molecules on the surface [32]. Furthermore, when describing the interaction between water and metal surfaces, van der Waals forces play a crucial role [31]. In particular, the non-local correlation effect has a significant impact on the adsorption of water on transition metal surfaces, while it is weaker on noble metal surfaces. This difference leads to the fact that although traditional semi-local functionals can roughly predict the adsorption structure of water, they are difficult to accurately reflect interface phenomena such as the formation of heterogeneous ice nuclei, which depend on long-range interactions. Therefore, explicit solvation models have advantages that implicit models cannot replace in revealing the complex physical and chemical behaviors of the reaction interface.

Although the above studies focused on the application of Pt-based materials in the ORR process, they also provided a reference for the dynamic ORR simulation of M-N-C materials. Similarly, the number of molecules in the solvation model established on the surface of the carbon-based catalyst has a significant impact on the accuracy of the simulation. For instance, Kirchhof et al. [99] conducted a calculation of the solvation energy on the graphene structure model doped with B (Fig. 4(a)). The results showed that the activity was relatively low when the solvation effect was not considered, which was significantly different from the experimental results. Furthermore, the author found that introducing different numbers (layers) of water molecules in the solvent model would have a significant impact on the calculation results (Fig. 4(b)). This further indicates that when the solvation model on the surface of the catalyst model is more refined, the predicted intrinsic activity values obtained are closer to the experimental results. However, the author also pointed out that currently, a hybrid simulation method needs to be developed, that is, using a lower theoretical level to conduct efficient simulations for more solvent molecules, while maintaining a higher theoretical level for the reaction molecules, their neighbors, and the catalyst to quickly obtain the thermodynamic intrinsic activity values that can accurately reflect the reaction environment. In addition to the non-metallic carbon-based materials, the M-N-C materials with FeN_4 sites have also been demonstrated [100]. The predicted potential of FeN_4 obtained through static calculation (0.61 V) deviates from the experimental observation results (Figs. 4(c) and 4(d)). However, when a solvation

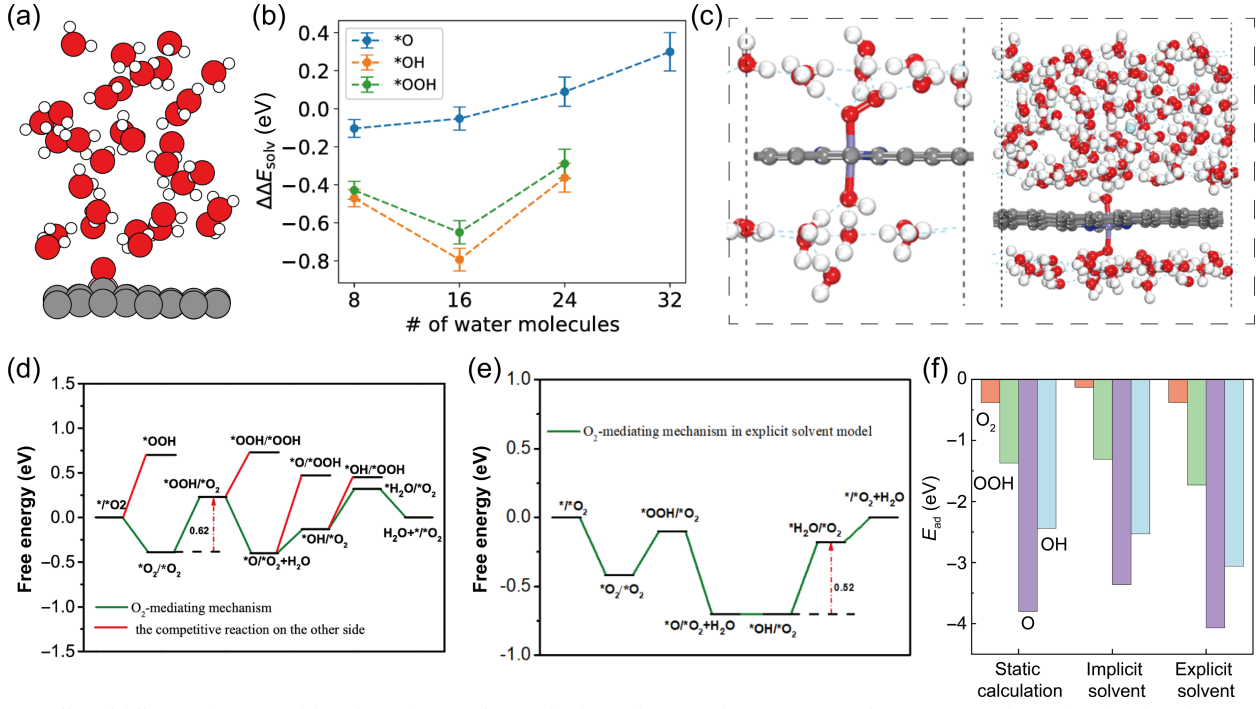

Figure 4 Effect of different solvation models at the catalyst interface on the thermodynamic adsorption energy of oxygen intermediates (a) B-doped graphene structure and surface solvent model. (b) The influence of the number of water molecules on the graphene-doped structure surface on the adsorption energy of oxygen-containing intermediates. Reproduced with permission from Ref. [99], © Kirchhoff et al. 2023. (c) Surface solvation models constructed at the FeN_4 site using the NEB method (left) and the constrained DFT-MD method (right). (d) The ORR free energy diagram of the FeN_4 site based on static calculations. (e) The ORR free energy diagram of the FeN_4 site calculated based on the explicit solvation model. Reproduced with permission from Ref. [100], © Elsevier B.V. 2025. (f) Comparison of adsorption energies of oxygen-containing intermediates under different solvation models. The data is sourced from Table 1 in the Ref. [100].

model is established, the limit potential increases to 0.71 V (Fig. 4(e)), and the intrinsic activity further improves and is in excellent agreement with the experimental values. This indicates that for M-N-C materials, it is very necessary to evaluate the influence of solvent effects on the adsorption energy of oxygen-containing intermediates (Fig. 4(f)). This can precisely reveal the thermodynamic intrinsic activity of potential ORR catalytic materials and help design better ORR electrocatalysts.

Based on this, theoretical researchers have developed many new simulation methods in recent years to establish explicit solvation models to obtain the intrinsic activity of M-N-C materials under the premise of reducing the computational cost as much as possible. For example, Chun et al. [33] developed a method for determining solvation enthalpy based on *ab initio* molecular dynamics (AIMD) sampling. They obtained the average value of the hydrated adsorbate-catalyst configuration through the simulated annealing process, and decomposed the solvation enthalpy into the energy combination of two sub-processes: water reorganization and adsorbate-solvent interaction (Fig. 5(a)). This method has been verified in the ORR Fe-N-C catalysts, significantly improving the processing accuracy of electrochemical interface energy. With the assistance of the explicit solvation model, not only can precise thermodynamic quantities (such as the adsorption energy of the oxygen intermediate and the change in reaction free energy) be obtained, but also the kinetics of the ORR process can be studied, such as the structural changes of surface water molecules. The hybrid solvent model proposed by Armillotta et al. [94] ingeniously combines the advantages of implicit methods and explicit methods. Based on a single-layer cobalt porphyrin as the model catalyst, they analyzed the formation and stability process of hydroxyl peroxide-water clusters in the presence of oxygen and water, and further demonstrated that the complex interactions among charge transfer, dipole–dipole interactions, hydrogen bonds, and solvation behavior jointly determine the ORR pathway. Wang et al. [101] combined classical MD and AIMD to construct an explicit water solvent to study the interface structure of the Fe-N_4-C catalyst (Fig. 5(b)). The study found that the structure of the interface water depends on the potential change. That is, when the potential shifts, the change in the structure of water molecules will further increase the number of hydrogen bonds. The hydrogenation of the oxygen-containing intermediate is less favorable at high potentials because the local water molecules are stabilized through hydrogen bonding and are away from the reaction center. This work reveals that the solvent on the catalyst surface has a significant impact on the adsorption of reaction intermediates at the FeN_4 active site during the ORR process. However, it should be pointed out that the improvement in the ORR kinetic performance is often the result of multiple factors (such as electron–proton transport, changes in RDS, reduction in activation energy, etc.). Merely regulating the structure or orientation of the interfacial water molecules to accelerate electron and proton transport during the ORR process cannot guarantee improved reaction kinetics.

In conclusion, by using the new dynamic density functional theory simulation method to establish a clear solvation model for M-N-C materials, we can effectively enhance our understanding of the ORR process by analyzing the changes in thermodynamic quantities and kinetic data under the solvation model. However, as mentioned by Wang et al., in addition to the solvent, the influence of potential is also very important and is usually inseparable from the establishment of the solvation model. In the following section, we will delve deeper into the impact of the applied potential on the dynamic process of ORR on M-N-C materials.

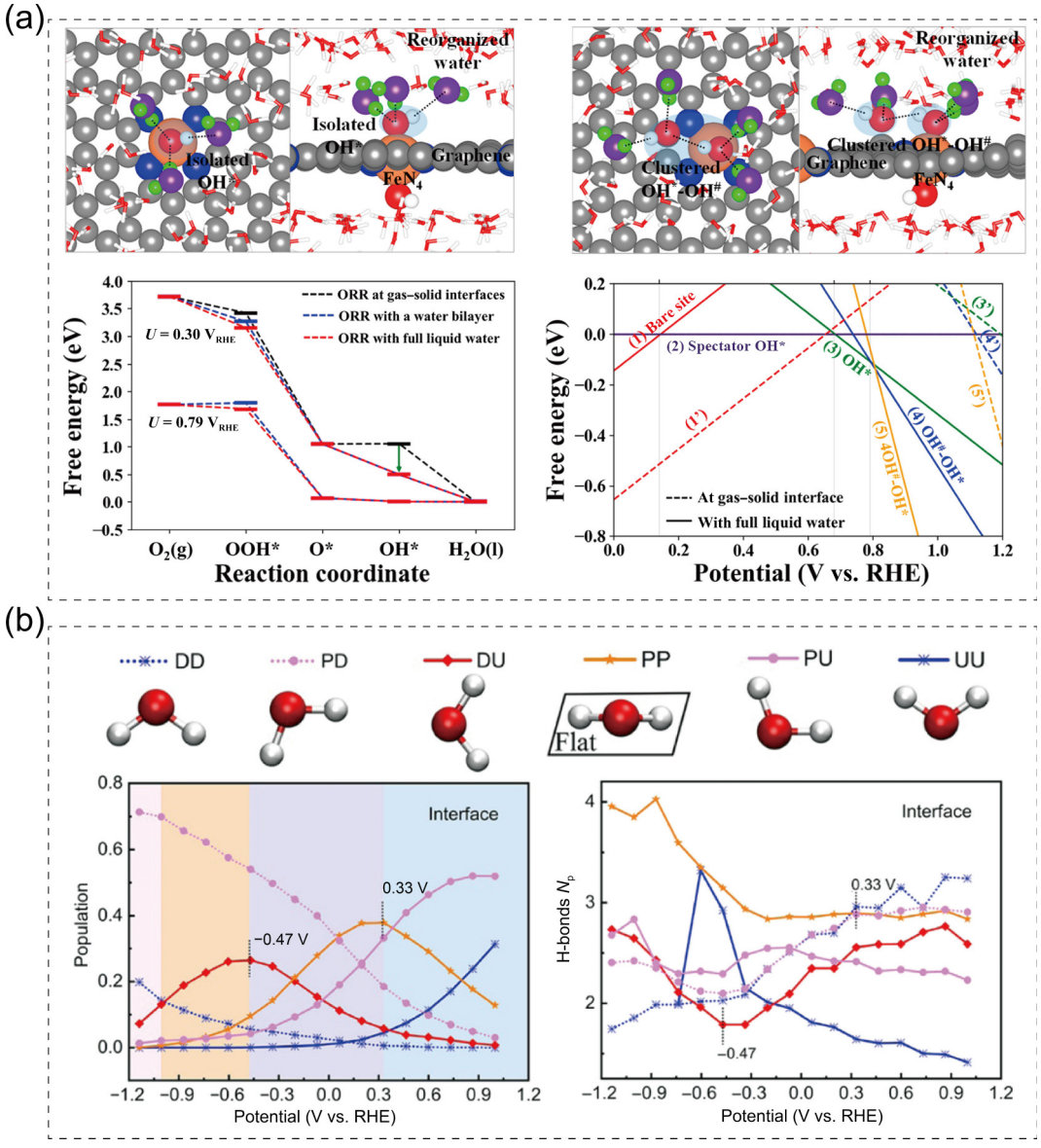

Figure 5 (a) Comparison of dynamic DFT calculation results and static DFT calculation results based on the display solvation model. Reproduced with permission from Ref. [33], © American Chemical Society 2024. (b) The evolution process of the structure of water molecules in the surface solvent model as the potential changes. Reproduced with permission from Ref. [101], © American Chemical Society 2023.

3.2 Applied potential on ORR

Practical electrochemical systems all operate under constant-potential conditions, while standard DFT calculations are usually carried out based on constant-charge conditions, this essential difference makes it impossible to directly obtain potential related reaction energy barriers and charge distributions through traditional calculations. This core challenge has directly promoted the development of the constant-potential DFT framework, whose core goal is to directly reflect the influence of applied potential in *ab initio* calculations. To overcome this limitation of the CHE model, Merand et al. [96] constructed a constant potential calculation framework based on density functional theory and achieved an accurate description of the electrocatalytic interface by fixing the chemical potentials of electrons and ions. Their research laid a solid theoretical foundation for the establishment of various related calculation schemes. At the specific implementation level of the constant potential method, Chen and Noskov [34] based on the proposed charge extrapolation method, could determine the relationship between the proton–electron transfer barrier and the potential with only one potential barrier calculation, and found that the transfer coefficient depends on the charge transfer amount from the initial state to the transition state. This simple and efficient method significantly reduces the computational cost of constant potential simulations, and thus has been widely applied in the kinetic study of ORR.

Similar to the discussion on the ORR electrolyte environment in the previous section, in this section we will separately analyze the influence of the applied potential on the thermodynamic and kinetic data of the M-N-C material during the ORR process. For the thermodynamic quantities in the ORR process, the adsorption energies of the three reaction intermediates often play a crucial role in the intrinsic thermodynamic activity of the material. In a recent study [102], when analyzing the influence of S-doped FeN_4 sites on the activity and stability of ORR, a constant potential implicit

solvent model was used to simulate the reaction environment. The calculation results showed that FeN_4S_1 had the highest theoretical ORR activity in a static environment, while in the constant potential implicit solvent model, FeN_4S_2 became the catalyst with the highest theoretical ORR activity. The enhancement of the intrinsic thermodynamic activity of FeN_4S_2 comes from the optimization of the adsorption energies of the three reaction intermediates (Fig. 6(a)). Although all the structural models employ the same calculation method, the results obtained can provide guidance for the trend of activity changes. However, this study only employed the implicit solvation model. The absence of real solvent molecules at the reaction interface may have a certain impact on the accuracy of the adsorption energy calculation. In contrast, Qin et al. [25] first conducted molecular dynamics simulations on the FeN_4C structure containing a displayed solvation model, and obtained a thermodynamically stable catalytic surface structure. Furthermore, based on the stable structure, the adsorption energies of oxygen-containing intermediates at the active center were calculated under the constant potential state and the neutral charge state, and the free energy changes (ΔG) for different reaction steps were also calculated. The results show that when there are different U values on the constant potential state, the ΔG values of the five oxygen reduction reaction steps change independently (Fig. 6(b)). This further indicates that the applied potential has different effects on the formation of reaction intermediates. It is worth noting that the changes or optimizations of these thermodynamic quantities can only indicate the trend of the inherent properties of the material, while the performance of the material in the experimental environment is often controlled by multiple factors.

Furthermore, the additional potential method also offers significant advantages for analyzing the stability of the ORR process in M-N-C materials. As shown in Fig. 6(c), Morankar et al. [103] constructed a thermodynamic phase diagram related to the ORR potential at the pyridyl FeN_4 site. The results indicated that the active site would adsorb a single OH group at 0.0 V. This configuration has the most favorable free energy within the potential range of 0.34 V (the purple area). Moreover, within the oxidation potential range of ORR, it still maintains a binding with iron but does not deactivate this site.

On the other hand, the applied electric potential also provides an effective approach for the study of the kinetic of M-N-C materials. In a previous study, Yu et al. [35] used the solvation model display and constant potential method to investigate the RDS of ORR at the FeN_4 active site. The authors found that RDS is the process where oxygen molecules replace the adsorbed water molecules on the iron, and the desorption of water molecules and the adsorption of oxygen occur simultaneously (Fig. 6(d)). The surface of the iron atom is not exposed. Moreover, this barrier will decrease as the electrode potential decreases. Differently, the latest study [30] indicates that the RDS of the ORR at the FeN_4 active site is related to the potential energy, rather than remaining constant within the effective potential energy range. When the applied electric potential is 0.0 V, RDS represents the desorption of $*H_2O$. As the electric potential increases (to 0.4 V), RDS transforms into the conversion

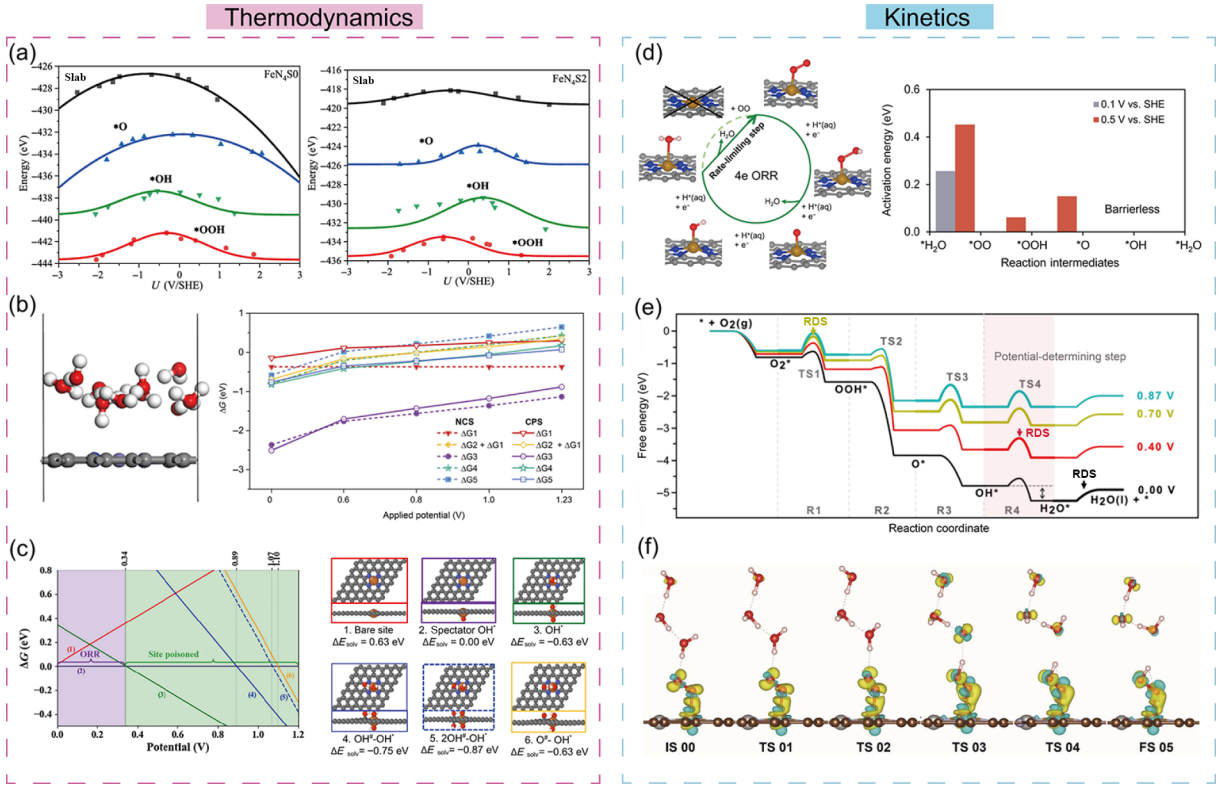

Figure 6 Study of ORR dynamic process under applied electric potential. (a) Adsorption models of adsorbed species at the FeN_4S_0 site and FeN_4S_2 under different applied potentials. Reproduced with permission from Ref. [102], © Elsevier B.V. 2024. (b) The explicit solvation model of the FeN_4 active site and the free energy change of the ORR process under different voltages. Reproduced with permission from Ref. [25], © American Chemical Society 2023. (c) Phase diagram for a pyridinic FeN_4 site in ORR. Reproduced with permission from Ref. [103], © Morankar, A. et al. 2023. (d) The ORR mechanism and the energy barriers for different reaction steps at different voltages. Reproduced with permission from Ref. [35], © American Chemical Society 2023. (e) The RDS transformation trend of ORR under different applied electric potentials. Reproduced with permission from Ref. [30], © American Chemical Society 2025. (f) The charge transfer of the catalyst in the proton transfer step of the ORR. Reproduced with permission from Ref. [104], © The Royal Society of Chemistry 2023.

of *OH to *H_2O, and eventually changes into the process of *O_2 being activated to *OOH (Fig. 6(e)). For single-atom catalysts like Fe-N-C, the RDS of the ORR is not constant. Early studies based on thermodynamic descriptors often concluded that the hydrogenation step was the RDS. However, DFT simulations based on constant potential suggest that the RDS strongly depends on the local solvation environment of the active site and the applied working potential. These studies collectively emphasize that to accurately understand and rationally design such catalysts, one must go beyond equilibrium-state thermodynamic analysis and conduct kinetic modeling in the explicit presence of potential and real solvents. However, it should be noted that the transformation of RDS does not guarantee an increase in the kinetic reaction rate. This is mainly related to factors such as activation energy and proton–electron transfer rate. For instance, Tamtaji et al. [104] conducted a study on the ORR mechanism and kinetics of the iron-nickel dual-atom catalyst based on constant potential DFT (Fig. 6(f)). The results showed that during the proton transfer process, the charge transfer and spin density of iron reached their maximum values. Moreover, when the potential relative to the standard hydrogen electrode (RHE) is greater than 0.25 V and less than 0.25 V, *OH and *O are respectively the main intermediates.

In this section, we discussed the influence of the applied electric potential on the thermodynamic and kinetic quantities of the M-N-C material in the dynamic study of ORR. In the following, we will discuss the pH dependence and ionic effects in the ORR process.

3.3 pH dependence and ions effects on ORR

As we discussed in the previous two sections, by constructing a solvent model on the catalyst surface and considering the applied electric potential, the thermodynamic and kinetic quantities of the material during the ORR process can be obtained. This provides a platform for researchers to further investigate the ionic effects and pH dependence of M-N-C materials in ORR [21, 29, 36–38, 47, 97, 105–110]. Therefore, in this section, we have discussed the latest research on the pH-dependence and ionic effects of M-N-C materials in recent years, with the aim of providing references for researchers.

For pH dependence, the static pH-modified method and molecular dynamics simulation can be used. For instance, the study by Li et al. [107] suggests that the strong pH value effect on ORR activity is due to the lower dissociation energy of the HO–OH bond in an alkaline environment, which subsequently leads to an increased rate of the H_2O_2 reduction reaction. The author obtained the ORR free energy diagrams at pH = 1 and pH = 13 by adding pH correction parameters to the static DFT calculations, and used this as a theoretical basis to explain the pH dependence of the MnN_4 site. However, the absence of the solvation model has rendered the results of this study not universally applicable. In contrast, the research conducted by Zhang et al. [36] is more comprehensive. By analyzing over 100 M-N-C structures and over 2000 sets of energy data (Fig. 7(a)), they discovered that the active volcano map of ORR would evolve with changes in pH value. Furthermore, they conducted molecular dynamics simulations based on the solvation model and the applied electric potential. The results indicated that the pH dependence of the M-N-C catalyst originated from its moderate dipole moment, the polarity of the adsorbate, and the proportional relationship between the oxygen-containing intermediates. The acid trap concept proposed in this study (Fig. 7(b)) provides significant reference value for the development of M-N-C type ORR catalysts.

The two aforementioned studies are more inclined to explore the effects of different pH values on the thermodynamic parameters of the ORR process. The research conducted by Men et al. [108] focused on the differences in the surface water molecule network near the active sites under different pH values. The author discovered that in an alkaline medium, when active metals adsorb oxygen intermediates, the hydrogen atoms in the structure of water molecules on the surface tend to be closer to the oxygen atoms (Fig. 7(c)). However, in acidic media, the orientation of the hydrogen atom exhibits the opposite characteristics (Fig. 7(d)). The orientation of water molecules in the solvent regulates the adsorption of the oxygen intermediate, and this may result in a pH dependent behavior. Furthermore, based on this discovery, the author expanded upon the ionic effect of ORR. It further reveals the source of the difference in acid-base activity of protic ionic liquids in the ORR process.

The above study not only revealed the possible reasons behind the pH dependence through molecular dynamics simulations, but also explored the ionic effects. The influence of ions on the activity regulation of ORR is also very important, especially for lithium-oxygen batteries. For instance, Chen et al. [106] systematically investigated the interaction between the CoN_4 site and the electrolyte during the ORR process using the AIMD method. The results indicate that the lithium-solvent bonding strength follows the order of donor quantity, which may lead to differences in the free energy of the interface reaction. The author believes that atomic-level cation affinity can be regulated through coordination engineering, and it can also be achieved by adjusting the solvate of the electrolyte to balance the interaction between cations and solvents. Subsequently, the research on the ORR cationic effect was further explored in a more comprehensive and in-depth manner in the work of Tian [109]. The author discovered through constant potential DFT combined with AIMD that lithium ions, sodium ions and potassium ions, etc., among the cations, would promote the pseudo-outer-surface oxygen reduction reaction mechanism during the ORR process (Fig. 7(e)). That is, the adsorbed water molecules on the surface act as dynamic bridges, simultaneously mediating the interface electron transfer and proton transport (Fig. 7(f)). The proposal of this reaction mechanism breaks through the traditional catalyst surface and overcomes the spatial limitations.

The above series of studies collectively indicate that the accurate description of the electric double layer effect is a core prerequisite for in depth understanding of electrochemical interface processes and realization of rational catalyst design. We then summarize recent studies on dynamic ORR processes, categorizing them based on the dynamic DFT methods employed and their research focus (Table 1). From the early simple electrostatic interaction models to the current complex theoretical systems that can self consistently handle electronic structures, defect formation, and ion distribution, the continuous progress of computational methods has enabled us to accurately reveal the physical essence of pH dependence and ion effects at the atomic scale, providing a solid foundation for the design and development of the next generation of high efficiency electrocatalytic systems. In summary, the inherent dynamic characteristics of electrochemical interfaces require theoretical simulations to break through the limitations of static vacuum approximation and realize the organic integration of electrolyte environment, constant-potential conditions, and ion effects. Currently, the integrated application of implicit and explicit

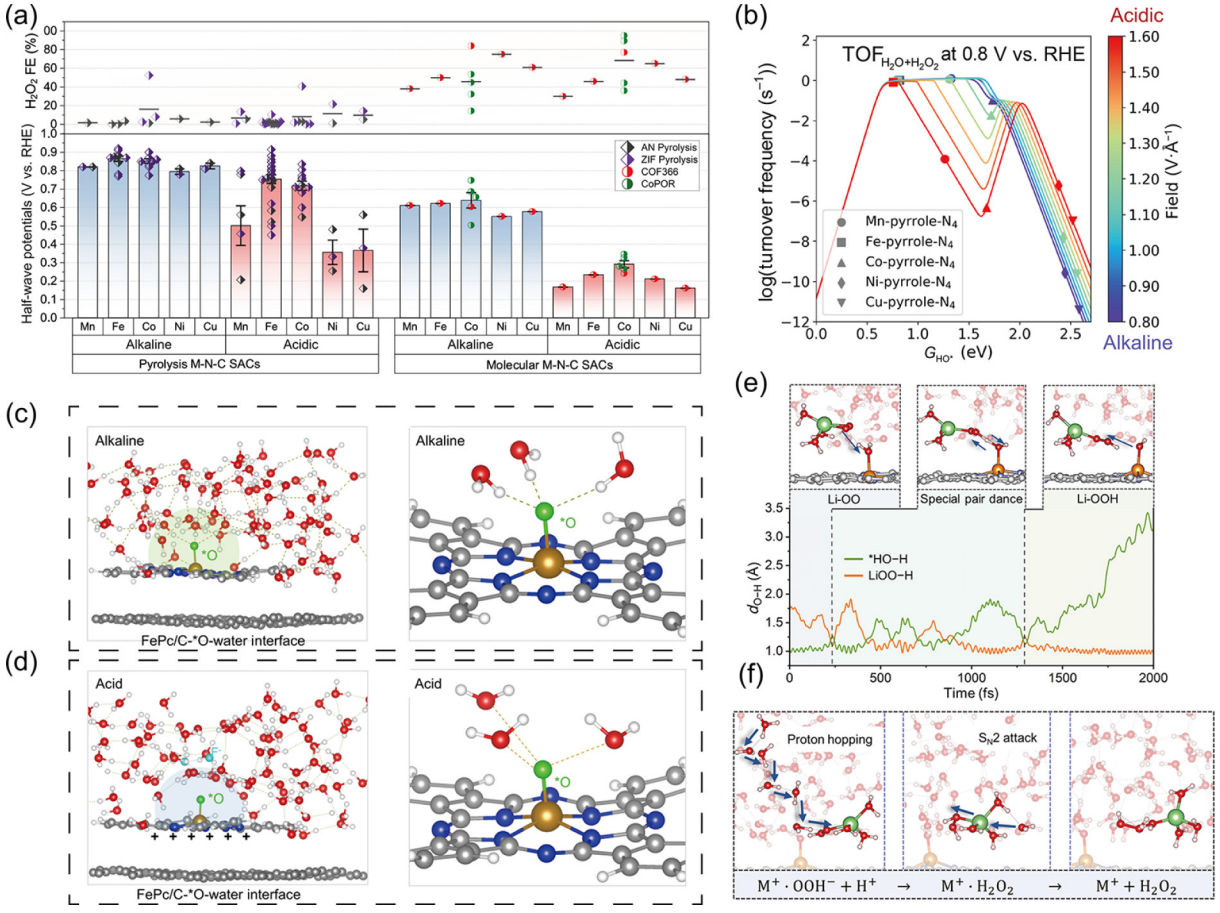

Figure 7 Study of dynamic ORR process under pH dependence or ion effects. (a) The influence of the active site types of M-N-C materials at different pH values on the ORR mechanism. (b) Activity volcano for the overall ORR TOF of M-pyrrole-N catalysts at 0.8 V/RHE. Reproduced with permission from Ref. [36], © Zhang, D. et al. 2024. (c) and (d) The solvation model of FePc in acidic and alkaline media and the corresponding structural evolution of water molecules in the solvent. Reproduced with permission from Ref. [108], © Dalian Institute of Chemical Physics, Chinese Academy of Sciences 2026. (e) The variation over time of the distance between the water molecules adsorbed by hydrogen atoms and the oxygen atoms in the lithium-oxygen complex. (f) Snap shots of key stages during the reaction process. Reproduced with permission from Ref. [109], © American Chemical Society 2025.

solvation models, the continuous development of constant-potential DFT calculation frameworks, and the continuous deepening of electric double layer theory are collectively promoting us to gradually uncover the atomic-level mechanism of electrochemical interface processes. The future advancements in machine learning-driven molecular dynamics simulations and innovative cross-scale computational methods will further facilitate breakthroughs in this field, providing a more solid theoretical foundation for the precise design of efficient electrocatalysts.

3.4 Spin-state dynamics for ORR

Recently, as researchers have gained a deeper understanding of the MN_4 site during the ORR process, the changes in the spin state of the metal have also become increasingly clear [111]. The intrinsic activity of ORR is believed to be related to the spin states of the d orbitals of the active metal [112, 113]. With the proposal of various dynamic DFT simulation methods, the dynamic evolution process of the active metal spin state during the ORR process has been further discussed. In this section, we will discuss the spin-state dynamics of ORR from two aspects, namely the spin-state evolution based on different oxygen intermediates [114–116] and the spin-state dynamic changes based on constant potential DFT [25, 117–119].

For the MN_4 site, the adsorption of different oxygen-containing intermediates by active metals is believed to occur in different processes of the ORR. Moreover, investigating the spin state changes after the metal forms bonds with different oxygen intermediates can effectively analyze the evolution of the spin state during the ORR process. For instance, Cheng et al. [114] combined FePc with Eu_2O_3 to enhance the spin state of the Fe center and the ORR performance through the f-p-d gradient orbital coupling. The author calculated the spin states of Fe after adsorption of three oxygen-containing groups and found that the Fe center coupled with Eu_2O_3 gained enhanced spin states, which further strengthened the bond order of the adsorbed *OOH groups (Fig. 8(a)). This facilitates the dissociation of the O–O bond, thereby providing potential support for the enhancement of the ORR kinetics. Mei et al. [115] also conducted a similar study. They used covalent organic framework materials as the ORR catalyst and calculated the bond sequences after Co adsorbed different intermediates. They also reached the same conclusion, that the enhancement of spin states would increase the calculated bond order values, which might be the reason why different materials exhibit different ORR activities. However, the difference is that the bond order of *OOH calculated by Mei et al. remained unchanged, while those of $*O_2$, *O, and *OH all increased (Fig. 8(b)). Interestingly, this is exactly the opposite of the calculation results of Cheng et al. This indicates that although the materials are all of the M-N-C type and all have the MN_4 active

Table 1 Summary of different dynamic DFT research methods and their focused areas

Research object	Electrolyte environment	Applied electric potential	pH dependence/ ions effects	Research focus	Refs.
B-doped graphene	√Implicit explicit	—[a]	—	Solvent model size on calculation accuracy	[99]
Fe-N-C	√Implicit explicit	√[b]	—	Adsorption of reaction intermediates	[100]
Fe-N-C	√Explicit	—	—	The stability of adsorption oxygen species	[33]
Co-N-C	√Explicit	—	—	The stability of adsorption oxygen species	[94]
Fe-N-C	√Explicit	√	—	Water molecule structure and adsorption energy	[101]
$FeCoN_6$	√Explicit	√	—	Dynamic evolution of active structures	[27]
Fe_2N_6	√Explicit	—	—	Dynamic evolution of active structures	[120]
M-N-C	√Implicit	√	—	Adsorption of reaction intermediates	[23]
Fe-N-C	√Explicit	√	—	RDS (non-electron transfer)	[25]
Fe-N-C	√Explicit	√	—	Adsorption energy and reaction free energy	[95]
$FeNiN_6$	√Implicit	√	—	Proton and electron transfer	[104]
FeN_4S_X	√Implicit	√	—	Adsorption of reaction intermediates	[102]
Fe-N-C	—	√	—	Dynamic structure of the active site	[103]
Fe-N-C	√Explicit	√	—	RDS (non-electron transfer)	[35]
Mn-N-C	√Implicit	—	√	pH-dependence	[107]
M-N-C	√Explicit	√	√	pH-dependence	[36]
FePcProtic ionic liquid	√Explicit	√	√	pH-dependenceIons effects	[108]
Co-N-C	√Explicit	—	√	Ions effects	[106]
Zn-N-C	√Explicit	√	√	Ions effects	[109]
Fe-N-C	—	√	—	Spin-state dynamics	[117]
Ru-N-C	—	√	—	Spin-state dynamics	[118]

[a]Dynamic DFT not used; [b]dynamic DFT used to account for reaction environment.

site, the differences in the active metals and the surrounding carbon structures will lead to variations in the calculated results. Furthermore, what is even more important is that through the aforementioned methods, only the spin behaviors of materials with different spin states in the specific ORR process can be compared horizontally. However, when the research object is the same material, it is extremely difficult to conduct a precise analysis of the spin state changes of active metals during the ORR process.

With the assistance of the constant potential DFT calculation method, the analysis of the spin states of the same material during the ORR process becomes possible. Zhan et al. [117, 118] have made many groundbreaking achievements in this field. They first constructed a typical FeN_4 site based on graphene [117], and calculated the projected density of states under constant potential DFT under different applied electric potentials. Based on the calculation results, the magnetic moment of the active metal Fe under different electric potentials was further calculated, which is considered to be closely related to the spin state. The results show that the magnetic moment of Fe significantly increases at 0.4 V and decreases at 1.2 V, which is related to the ORR potential (Fig. 8(c)). Meanwhile, the calculated number of electrons gradually decreases as the applied electric potential increases. This study clearly obtained the dynamic evolution process of the spin state of the active metal Fe at the FeN_4 site during the ORR voltage, providing new insights into the dynamic ORR process. However, it is worth noting that when the active metal changes, the spin state also varies differently. As shown in Fig. 8(d), Zhan et al. discovered in their latest research that when Ru acts as an active metal [118], the change in the magnetic moment of the metal during the ORR process is different from that of Fe. As the voltage increases, the magnetic moment continues to decrease, which is consistent with the trend of the change in the number of electrons. This indicates that when the structure of the active metal or the active site position changes [25], the analysis of the spin state evolution obtained through theoretical methods often involves uncertainty. This requires combining it with experimental data (such as characterization methods like hysteresis loops, Mössbauer spectra, etc.) to further reveal the dynamic process of the material in the ORR.

4 Critical evidence for dynamic processes: *in-situ* characterization

4.1 Probing dynamic active structures via *in-situ* XAS

In-situ XAS, encompassing XANES and EXAFS, is a core technique for unraveling the dynamic evolution of electronic and local structures of M-N-C catalysts during the ORR [119–125]. Unlike *ex situ* characterization that only captures static information, *in-situ* XAS enables real-time tracking of structural changes in metal active centers under working conditions, directly establishing the correlation between structural dynamics and catalytic performance. However, it is necessary to point out that although the *in-situ* XAS technique has been highly developed, the signal source of XAS is still averaged. For M-N-C materials, the structure of active center is difficult to remain consistent after high-temperature carbonization. This further makes it challenging to accurately reveal the geometric or electronic structure changes of the active center through XAS data.

The current ORR research on M-N-C materials is still

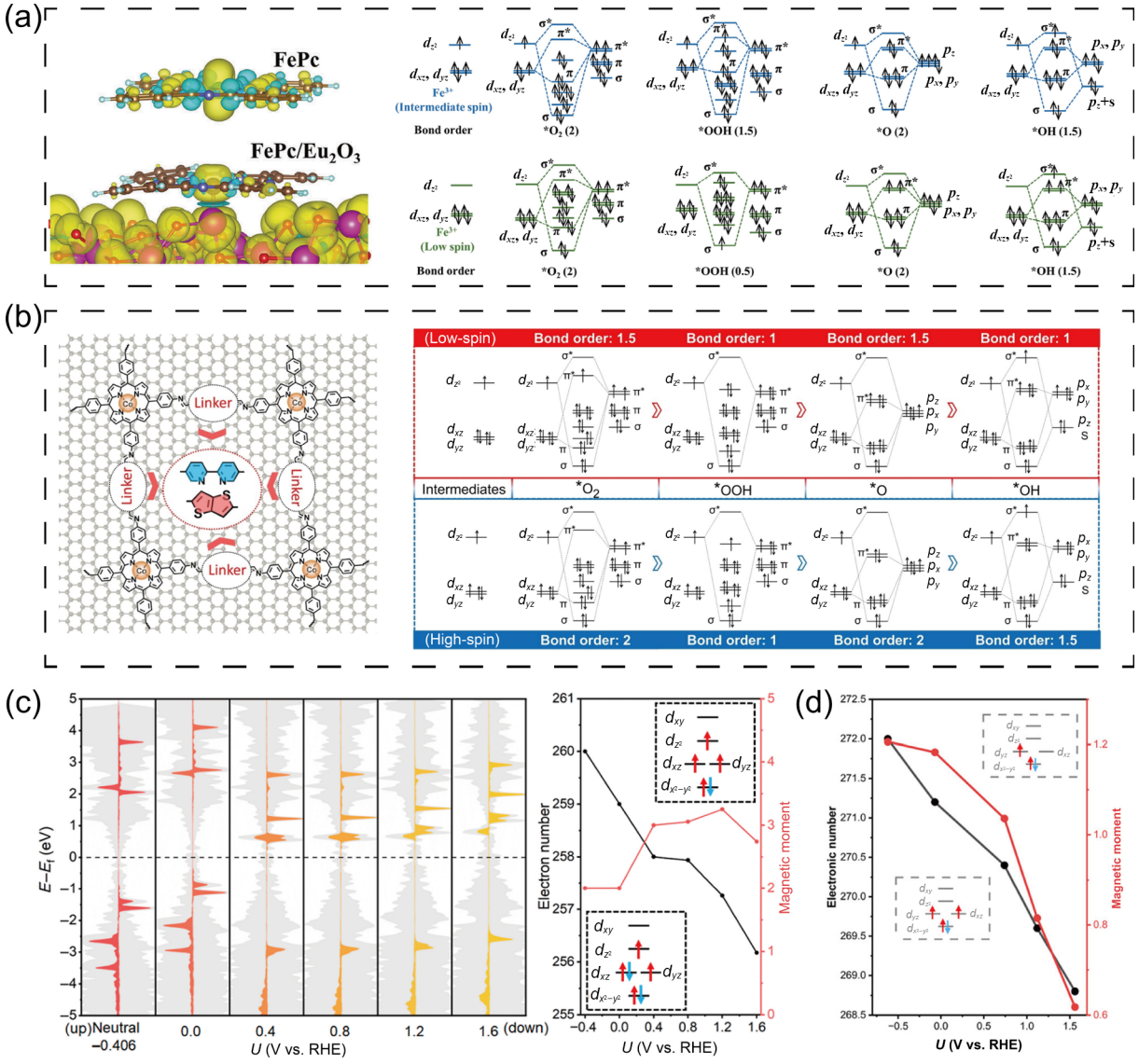

Figure 8 Spin-state dynamics during the ORR process. (a) The spin state and bond order changes of FePc/Eu_2O_3 materials after adsorbing oxygen-containing intermediates in the ORR process. Reproduced with permission from Ref. [114], © Cheng, R. Q. et al. 2025. (b) The spin state and bond order changes of N/S-COF@CNT materials after adsorbing oxygen-containing intermediates in the ORR process. Reproduced with permission from Ref. [115], © Wiley-VCH GmbH 2023. (c) In addition, the variation trends of the d orbital projection state density of Fe, the magnetic moment, and the number of electrons in the Fe-N-C material with respect to the applied electric potential. Reproduced with permission from Ref. [117], © American Chemical Society 2024. (d) The variation trends of the magnetic moment and electron number of Ru in the Ru-N-C material with the change of electric potential. Reproduced with permission from Ref. [118], © the Owner Societies 2025.

dominated by Fe-N-C. The latest research [121] indicates that the *in-situ* XANES data of Fe at the FeN_4 site shows a phenomenon of first shifting to the right and then to the left with the change of voltage (Fig. 9(a)). Near a voltage of 1.0 V, the X-ray absorption edge transitions to higher energy. This is mainly due to the combination of O_2 with the Fe sites, which in turn alters the oxidation state of Fe. Notably, this transition may not be observed in some materials, mainly because this process is very rapid and it is difficult to capture the signal. At low voltages, the absorption moves to lower energy, indicating that oxygen desorbs from the catalyst. Compared to a single FeN_4 site, many current studies focus on introducing additional metal atoms near the Fe site to form a dual-atom site. The first to be considered are Fe–Fe atom pairs, which may also be present in small amounts in single atomic Fe-N-C materials (since the structure after pyrolysis is uncertain). For instance, Li et al. [120] analyzed the bond length of Fe–N bonds through *in-situ* EXAFS. The results showed that the Fe–N bonds in the dual Fe sites remained almost unchanged, while the Fe–N bonds in the single Fe sites were stretched during the reaction process (Fig. 9(b)). The above results indicate that the introduction of additional metal atoms will further modify the geometric or electronic structure of the active Fe atoms during the ORR process. However, based on the average XAS signals of all types of Fe atoms, accurately describing this change in geometry or electronic structure remains a challenge.

For DACs, many metal combinations have already been explored. Here, we still take Fe-based DACs [122–124] as example to briefly discuss the role of *in-situ* XAS in the dynamic process of ORR. However, we found that the XAS data of Fe atoms was significantly influenced by the type of additional metal at the dual atom site. For instance, Zhang et al. [122] in their recent work introduced Sn as a secondary metal, thereby forming Fe–Sn dual

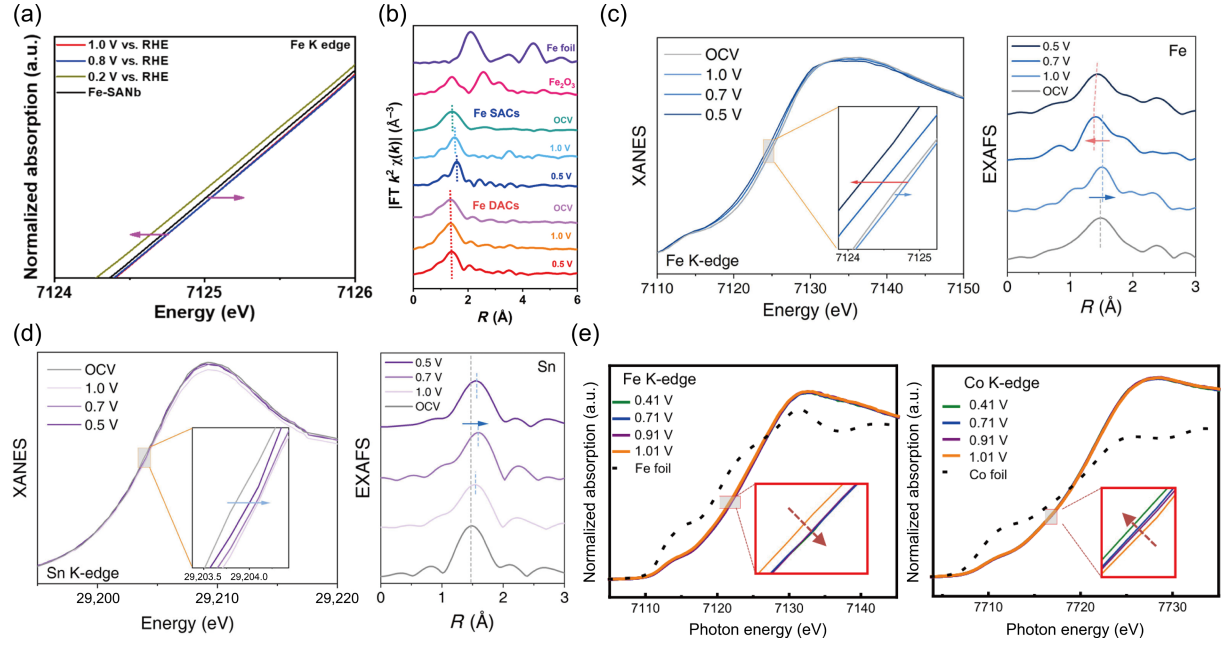

Figure 9 Study of ORR dynamic process via *in-situ* XAS. (a) *In-situ* XANES data of Fe atoms in Fe-SANb. Reproduced with permission from Ref. [121], © Elsevier B.V. 2026. (b) *In-situ* EXAFS spectra at the Fe K-edge under different potentials for Fe single atom sites and Fe-Fe dual atom sites. Reproduced with permission from Ref. [120], © Elsevier B.V. 2025. (c) and (d) *In-situ* XANES and EXAFS spectra at the Fe K-edge and Sn K-edge under different potentials for Fe-Sn dual atom sites. Reproduced with permission from Ref. [122], © Wiley-VCH GmbH 2026. (e) *In-situ* XANES and EXAFS spectra at the Fe K-edge and Co K-edge under different potentials for Fe-Co dual atom sites. Reproduced with permission from Ref. [123], © Yuan, L. J. et al. 2025.

atom sites. As shown in Fig. 9(c), the XANES and EXAFS of Fe exhibited a phenomenon of first shifting to the right and then to the left under the variation of voltage. This is consistent with the performance of Fe in single atomic sites [121]. It did not occur that the XAS data of the Fe-Fe diatomic sites synthesized by Li et al. [120] remained unchanged. This further indicates that the XAS data currently collected based on M-N-C materials has considerable uncertainty. In addition, the author also conducted *in-situ* characterization of the Sn atom at the Fe-Sn dual atom sites. The XAS data of Sn showed a consistent rightward shift as the voltage changed (Fig. 9(d)). When the secondary metal changes, such as when Co acts as the secondary metal and forms the Fe-Co dual atom sites [123], the *in-situ* XANES of the Fe atom is opposite to that of Co. It shifts to the right with the change of voltage, while Co always shifts to the left (Fig. 9(e)).

Furthermore, in the latest study, Song et al. [119] synthesized tri-metallic single-atom catalysts composed of Fe, Mn, and Zn metal atoms. However, through analyzing the *in-situ* XANES data, the author discovered that the energy of the absorption edge for all three metals exhibited a pattern of first increasing (moving to the right) and then decreasing (moving to the left) as the ORR voltage changed. This further demonstrates that the current XAS data based on the average atomic signals in the materials is unable to accurately reveal the dynamic change patterns of M-N-C materials during the ORR process. It is difficult to accurately reconstruct the dynamic evolution process of the active sites during the ORR process solely through *in-situ* XAS.

Although researchers can use *in-situ* XAS to analyze the geometric or electronic structure changes of the active metals in the M-N-C materials during the reaction, and compare the XAS data of different materials under the same standard to analyze the reaction mechanism or the dynamic structural evolution. However, for the M-N-C materials obtained through high-temperature carbonization, the structural uncertainty of the active sites greatly undermines the credibility of *in-situ* XAS in the study of dynamic ORR. This further demonstrates that the current research on dynamic ORR requires the combination of dynamic DFT simulation and *in-situ* characterization techniques.

4.2 Probing reaction pathways with *in-situ* Raman and *in-situ* FTIR

In this section, we will discuss the recent dynamic studies on the ORR of M-N-C materials using *in-situ* Raman and *in-situ* FTIR. Compared with *in-situ* XAS, which can reveal the geometric and electronic structure changes of a certain element in the material, *in-situ* Raman and *in-situ* FTIR can identify the types of groups adsorbed on the active sites. This undoubtedly clearly reveals the reaction mechanism of the material during the ORR process, especially for the active centers with complex structures. We will respectively discuss the roles of *in-situ* FTIR and *in-situ* Raman in revealing the ORR mechanism.

For *in-situ* FTIR, Lu et al. [22] prepared Fe and P atom-dispersed Fe,P/HPC catalysts (Fig. 10(a)) via a transition metal complex adsorption-thermal activation strategy. *In-situ* FTIR detected characteristic peaks at 1060 cm^{-1} (O_2^-), 1248 cm^{-1} (*OOH), and 3445 cm^{-1} (*OH) during ORR, confirming the formation of a stable hydrogen bond network between the Fe, P catalytic pairs and intermediates (Fig. 10(b)). The identification of reaction intermediates provided experimental evidence for the authors to propose the corresponding ORR mechanism. The above study demonstrates that *in-situ* FTIR can reveal the ORR mechanism and provide experimental explanations for the comparison of ORR activities of different materials. Furthermore, for the non-metallic nitrogen-doped carbon materials, Bhardwaj et al. first identified the characteristic peaks for superoxide ions and adsorbed O_2 molecules through *in-situ* attenuated total reflection-Fourier transform

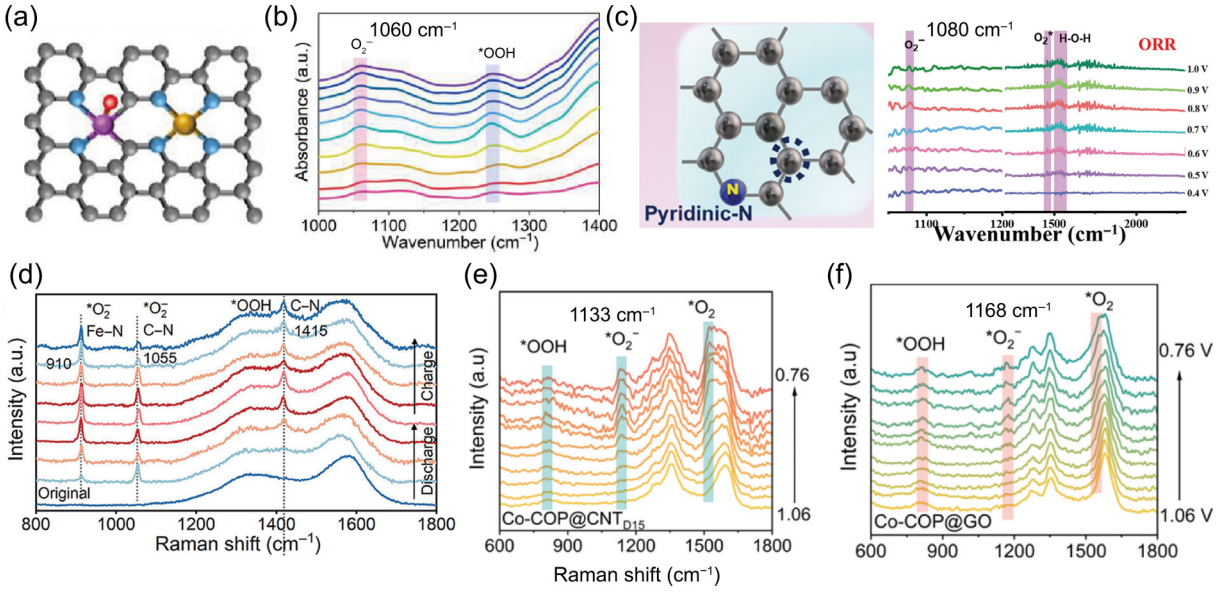

Figure 10 Study of ORR dynamic process via *in-situ* Raman/FTIR. (a) The structural model of Fe, P/HPC catalysts. (b) *In-situ* FTIR data of Fe, P/HPC at the ORR potential. Reproduced with permission from Ref. [22], © American Chemical Society 2025. (c) The structural model of non-metallic N-doped materials and the corresponding *in-situ* FTIR characterization. Reproduced with permission from Ref. [127], © Wiley-VCH GmbH 2025. (d) *In-situ* Raman characterization of Fe_2N/PR-Fe materials. Reproduced with permission from Ref. [126], © American Chemical Society 2025. (e) and (f) *In-situ* Raman characterization of Co-COP@CNT_{D15} and Co-COP@GO. Reproduced with permission from Ref. [128], © Elsevier B.V. 2025.

infrared spectroscopy (ATR-FTIR), which were 1080 and 1455 cm^{-1}, respectively (Fig. 10(c)). The identification of superoxide anions proved that the ORR followed the 4-electron transfer mechanism. Additionally, the author found the characteristic peak corresponding to the *OH group at 3300 cm^{-1}, indicating that water has already formed as a product. In the aforementioned study, the application of *in-situ* FTIR provided experimental evidence for the identification of the ORR mechanism, further supporting the construction of the static model based on DFT calculations. However, it must be acknowledged that the peak position of the functional group varies in different studies. For instance, the O_2^- exhibited characteristic peaks at 1160 and 1180 cm^{-1} in the two aforementioned works. This phenomenon is particularly common in the current ORR studies of M-N-C materials. The main reason for this is that carbon materials, under the reaction potential, not only react with the intermediate products but also adsorb other types of oxygen-containing intermediates, which interfere with the signal capture of *in-situ* FTIR. This situation also frequently occurs in *in-situ* Raman spectroscopy.

Wang et al. [126] used the heterojunction catalyst (Fe_2N/PR-Fe SA) designed by them to deeply track the evolution process of the ORR intermediates through *in-situ* Raman spectroscopy technology. During the ORR process, the Fe–N sites exhibited the characteristic peak of O_2^- (910 cm^{-1}), while at the C–N sites, the characteristic peaks of O_2^- (1055 cm^{-1}) and OOH (1415 cm^{-1}) were observed (Fig. 10(d)). The synergistic effect of this heterostructure regulated the electronic structure of the Fe atoms and accelerated the desorption of OH in the ORR process. The presence of O_2^- is generally regarded as a key feature of the 4-electron ORR. However, in another study, the peak position of O_2^- differs significantly from that of Wang et al. The *in-situ* Raman spectroscopy characterization results conducted by Zhang et al. [128] on the Co-COP@CNT_{D15} and Co-COP@GO catalysts revealed that Co-COP@CNT_{D15} exhibited a characteristic peak at 1133 cm^{-1} corresponding to the O–O bond stretching vibration in O_2^- at a potential of 0.97 V, while Co-COP@GO required a lower potential (0.92 V) to observe a similar signal at 1168 cm^{-1} (Figs. 10(e) and 10(f)). In both of these studies, the appearance of O_2^- during the ORR process was analyzed using *in-situ* Raman spectroscopy. However, there were significant differences in the peak positions.

In conclusion, *in-situ* Raman and *in-situ* FTIR spectroscopy have provided experimental evidence for the identification of the reaction mechanism in the dynamic study of ORR, but the peak positions of the characteristic peaks are difficult to be unified. The shift of these characteristic peaks is mainly due to the fact that the M-N-C material has difficulty maintaining a clean and ideal catalytic reaction surface during the ORR process. The dynamic DFT simulation can establish a relatively idealized catalytic reaction surface by taking into account the environmental factors such as solvents and potentials during the ORR process. Therefore, combining dynamic DFT simulation with *in-situ* characterization techniques can provide comprehensive insights into the dynamic study of ORR.

4.3 Visualizing dynamic evolution with atomic resolution via scanning tunneling microscopy (STM)

Currently, the application of *in-situ* electron microscopy (primarily STM) in ORR research of M-N-C catalysts is limited. However, its atomic-level spatial resolution enables direct visualization of nanoscale structural dynamics and active site behavior, making it a key tool for resolving reaction mechanisms and degradation pathways [26, 57, 129, 130]. Through *in-situ* observation of model M-N-C catalysts such as metal porphyrins/phthalocyanines, researchers have captured multi-dimensional core information. At the single-molecule level, both CoTPP/Au(111) system [26] and FePc/Au(111) system [57] confirmed that M-N_4 sites can form reversible complexes with O_2 via potential regulation high contrast bright spots (CoTPP-O_2/FePc-O_2) appeared in STM under O_2 saturation, and the bright spots turned into low-contrast metal porphyrin/phthalocyanine molecules when the potential was

reduced to the ORR range (−74 mV/50 mV); furthermore, DFT simulations of the FePc system further verified that this signal originates from enhanced orbital overlap between Fe and O_2. Friesen et al. [129] found that the electron-donating effect of highly oriented pyrolytic graphite (HOPG) supports enables cobalt octaethylporphyrin (CoOEP, which does not bind to O_2 at room temperature) to form stable CoOEP-O_2 complexes (characterized by low STM contrast); combined with Langmuir analysis, the half-saturation pressure of O_2 ($P_{1/2}$) at 298 K was obtained as 3200 Torr, revealing the regulatory role of supports in the O_2 binding capacity of metal centers. At the degradation behavior level, Hulsken et al. [130] observed paired Mn(IV)=O species (paired bright spots in STM) formed by O_2 homolysis in the Mn/Au(111) system, which aggregated into 2–3 nm Mn clusters after long-term reaction; Cai et al. [26] also found that after potential cycling of CoTPP, Co–N bond cleavage led to Co^{2+} leaching and redeposition as < 1 nm particles, simulating the metal leaching degradation of real M-N-C catalysts. In addition, the interfacial effect of supports was clearly revealed: HOPG stabilizes CoOEP-O_2 complexes through electron donation and maintains structural integrity after long-term ORR; Au(111) induces Mn(III) → Mn(II) reduction of Mn via axial coordination, both confirm that supports can enhance catalyst stability.

Current *in-situ* electron microscopy research still faces challenges: It is mostly limited to model catalysts; the low metal loading of real Fe-N-C makes signal capture difficult; The electrolyte thickness in liquid cells deviates from practical operating conditions; STM has limited applicability to insulating carbon supports. Future efforts need to make breakthroughs in three aspects: developing high-sensitivity *in-situ* scanning transmission electron microscopy (STEM, combined with energy-dispersive spectroscopy); optimizing liquid cell design; combining with other characterization techniques to achieve simultaneous morphology-electronic state analysis.

5 Bridging dynamic simulations with *in-situ* characterization

Although dynamic DFT calculations and *in-situ* characterization techniques have demonstrated significant value in understanding the dynamic processes of the ORR and monitoring reaction intermediates in real time, respectively, they are still largely applied independently in ORR mechanistic studies. The synergistic integration of these two approaches has not yet been adequately explored. Indeed, combining dynamic simulations with *in-situ* experimental data enables mutual validation and complementarity between theoretical models and experimental observations, thereby providing a more comprehensive and reliable understanding of the dynamic behavior and active site evolution in electrocatalytic processes [59–62, 108, 110, 120, 122, 131–133]. The following section will briefly discuss the integrated application of dynamic DFT simulations and *in-situ* characterization techniques in ORR and other electrocatalytic reaction.

5.1 Dynamic DFT and *in-situ* characterization for ORR

Regarding the study of carbon-based materials in the ORR process, some researchers have gradually realized recently that combining dynamic DFT simulation and *in-situ* characterization techniques can deeply reveal the essential reasons for the activity changes of materials in different media. For instance, Li et al. [61] used the $FeCoN_6C$ dual-atom catalyst as a model, and through AIMD simulation, they constructed the alkaline (pH = 13) and acidic (pH = 1) reaction interfaces under a constant potential condition. The simulation results indicate that the charge state on the catalyst surface remains almost unchanged under the reaction potential in an alkaline environment, but becomes strongly positively charged in an acidic environment (Fig. 11(a)). This leads to the ability of disordered water molecules in the alkaline environment to form hydrogen bonds with the surface oxygen intermediates, promoting proton-coupled electron transfer. In the acidic environment, the strong electric field polarization disrupts the hydrogen bond network, increasing the proton transfer barrier. Further *in-situ* characterization proves that the O–H stretching vibration peak of the interface water at the alkaline environment is located at 3200 cm^{-1}, corresponding to a strong hydrogen bond interaction. In the acidic environment, this peak shifts to 3400 cm^{-1}, indicating that the hydrogen bond network has been disrupted (Figs. 11(b) and 11(c)). This work, by combining dynamic DFT simulation and *in-situ* characterization, for the first time clarifies that the interface microenvironment is the core origin of the pH-dependent activity of ORR on M-N-C materials, rather than the reaction thermodynamic barrier obtained from static simulation. Furthermore, the non-metallic nitrogen-doped carbon materials (NGMs) also show a significant pH-dependence in the ORR application. Unlike Li et al., who conducted their research based on the $FeCoN_6$ structure with a clear active site as a model, the identification of the actual active sites has always been a challenge for the design of NGMs materials. Based on this, Bai et al. [133] prepared a group of model catalysts with precisely controllable active sites. Using constant potential DFT, they investigated the activity change trends of the model catalysts at different potentials under different pH conditions. Combined with *in-situ* attenuated total reflection-surface enhanced infrared spectroscopy (ATR-SEIRAS), it was proved that under strong acidic conditions, the nitrogen-doped sites and the adjacent carbon atoms did not have significant ORR activity, while the edge defects were the main pH-agnostic active sites, which could directly decompose O_2 molecules in acidic, alkaline and neutral conditions, especially in acidic media.

The above two research cases respectively conducted pH dependence studies on the two materials, M-N-C and NGMs, revealing the intrinsic sources of catalytic activity of carbon-based materials under different reaction media. While Men et al. [108] modified the reaction medium and used protonic ionic liquids to investigate the pH-dependence of FePc in the ORR process. Studies have shown that the evolution behavior of ORR activity caused by proton-type ionic liquid modification exhibits a clear pH dependence. Through molecular dynamics simulation and *in-situ* surface-enhanced infrared absorption spectroscopy, this phenomenon is attributed to the regulatory effect of ionic liquid modification on the distinct electrochemical interface structures under acidic and basic ORR conditions. That is, proton-type ionic liquids with lower pKa values will bring higher acidic ORR activity.

In addition, the combination of dynamic DFT and *in-situ* characterization can also provide strong theoretical support and evidence for the development of new materials for ORR. For instance, Zhang et al. [131] proposed an optimization strategy for the Lewis acid-mediated interface process to enhance the ORR performance of FePc. The author constructed MoS_2 beneath FePc to form Fe–S bonds (Figs. 11(d)–11(f)). The change in site acidity improved the interface water molecule network, thereby enhancing

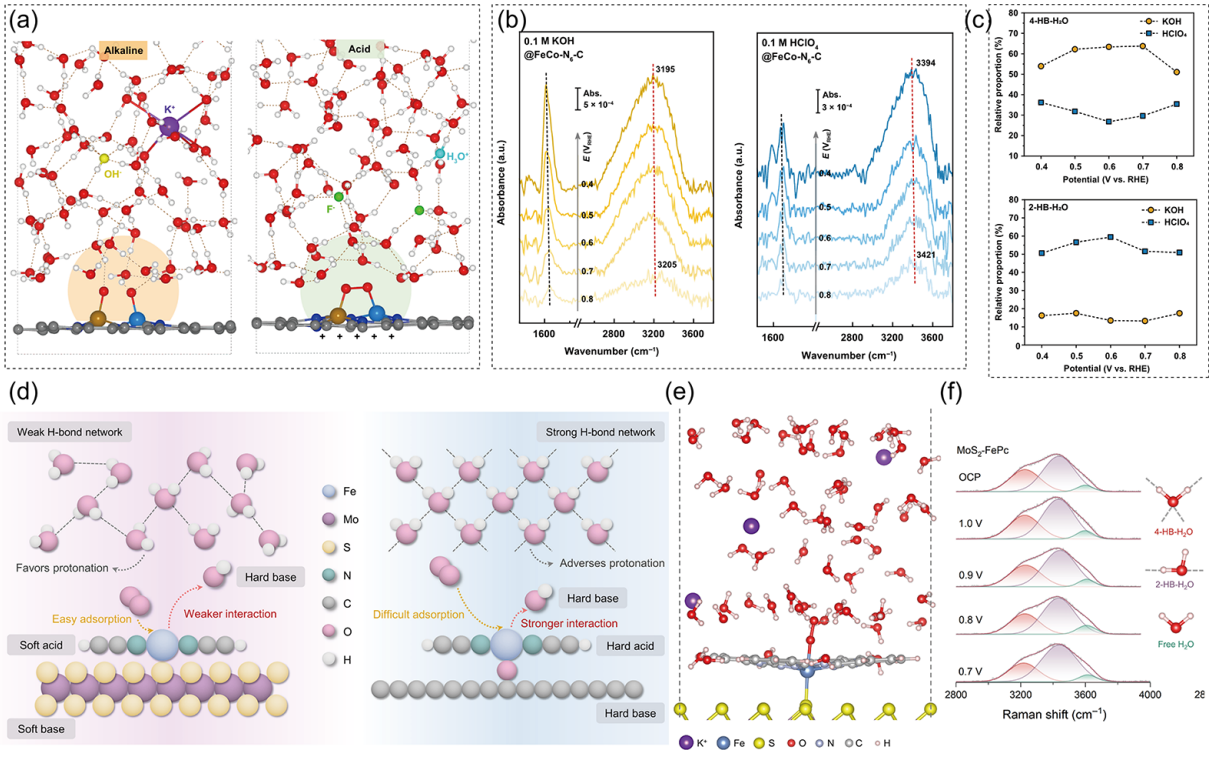

Figure 11 Study of dynamic process of electrocatalytic reaction combined with dynamic DFT and *in-situ* characterization. (a) The adsorption of O_2 by FeCo-N_6-C active center under solvation model and acid-base ion effect is shown. (b) *In-situ* SEIRAS characterization of FeCo-N_6-C catalyst under acidic and alkaline conditions, respectively. (c) Analysis of interfacial water molecule types of the catalyst under acidic and alkaline conditions respectively. Reproduced with permission from Ref. [61], © Li, P. et al. 2023. (d) Schematic illustration of the interfacial mass transport and electron transfer process accelerated by Lewis acid mediation. (e) The interfacial structures at ORR potentials on the O_2 adsorbed electrode surfaces for FePc/MoS_2. (f) Deconvolution of the O–H stretching peak into three components. Reproduced with permission from Ref. [131], © Elsevier Ltd. 2025.

the transmission of reactive oxygen species and promoting the subsequent protonation process, thereby increasing the ORR catalytic activity.

As mentioned above, the dynamic DFT combined with *in-situ* characterization plays a significant role in revealing the intrinsic activity regulation mechanism of M-N-C materials for ORR and in the development of new materials. It can be foreseen that this method may contribute to the research on improving the stability of M-N-C materials in real reaction environments.

5.2 Dynamic DFT and *in-situ* characterization for other electrocatalytic reaction

In addition, for other types of electrocatalytic reactions, the combination of kinetic simulations and *in-situ* characterization techniques also offers advantages in in-depth mechanistic investigations. Here, we will briefly discuss the breakthroughs achieved through this strategy in other types of electrocatalytic reactions, hoping to provide more ideas for improving the activity of ORR and developing new materials.

For example, in the case of the hydrogen evolution reaction (HER) and nitrogen reduction reaction (NRR), Wang et al. [62] conducted a molecular dynamics simulation to study the solvation behavior of high-concentration lithium chloride electrolyte. They found that lithium ions formed a rigid hydration shell with water through strong Coulombic interactions. This inhibited the activity of water as a proton source, and further induced the non-uniform nucleation and enrichment of nitrogen gas at the catalyst interface. Subsequently, *in-situ* X-ray diffraction results showed that in a 10 M LiCl solution system, the carbon characteristic diffraction peaks of the catalyst gradually weakened as N_2 adsorption proceeded. This confirmed the enrichment phenomenon of N_2 at the interface, which also corroborated the results of the molecular dynamics simulation. Although this work focuses on the NRR reaction, its main conclusions can provide a reference for the development of ORR catalysts in PEMFCs, as the rapid diffusion of water molecules in the catalytic layer is also of great significance.

Furthermore, the stability of the electrocatalyst is of crucial importance for its industrial application. Unfortunately, the stability of M-N-C materials in energy conversion devices such as PEMFCs still needs to be significantly improved at present. For the improvement of stability, Chang et al. [59] combined molecular dynamics simulation with *in-situ* characterization to elucidate the mechanism of the increase in material stability. Based on this, the authors dynamically constructed a dense oxide layer on nickel molybdate, forming an effective protective barrier to prevent the loss of molybdenum and enhance the stability of the material. This catalytic material was able to operate stably at a current density of 0.45 A·cm^{-2} in an industrial alkaline electrolyzer for 1400 h.

Studies on different systems have shown that the advantage of kinetic simulations lies in revealing the regulatory laws of the interfacial microenvironment (pH, cations, solvation) on reaction pathways and energy barriers at the atomic scale, while *in-situ* characterization can real-time capture the structural evolution and intermediate behavior during the reaction. The synergy between the two not only verifies the reliability of simulation results but also identifies key factors not considered in simulations (such as the reconstruction of active sites and dynamic transformation of

intermediates in actual reactions), providing comprehensive and accurate theoretical and experimental support for the structural design and performance optimization of electrocatalytic materials. We subsequently summarized recent studies that integrate dynamic DFT and *in-situ* characterization for analyzing electrocatalytic reaction processes, categorizing them according to the dynamic DFT methods employed, the *in-situ* characterization techniques utilized, and the key advancements achieved (Table 2).

6 Summary and outlook

6.1 Summary

M-N-C catalysts, leveraging the advantages of atomically dispersed metal coordination sites, high catalytic activity, and low cost, have emerged as one of the most commercially promising catalytic materials in the field of ORR. The core of their catalytic performance depends on the geometric structure, electronic state properties of active centers, and their dynamic evolution during reactions, and the analysis of these key pieces of information has always relied on the synergy between theoretical calculations and experimental characterization.

Currently, DFT calculations remain the core tool for revealing the microscopic mechanism of M-N-C catalysts, playing an irreplaceable role in predicting active center configurations, calculating intermediate adsorption energies, and analyzing the thermodynamics of reaction pathways. However, it should be clarified that most traditional DFT studies are based on idealized static models and fail to fully reproduce the complexity of the real ORR environment: On the one hand, they ignore the solvation effect of solvent molecules in the electrolyte, leading to deviations between the calculated key parameters of active sites and experimental observations; on the other hand, they do not consider the constant potential conditions and dynamic charge transfer during the reaction, making it difficult to simulate potential-dependent electronic state evolution, spin crossover effect, and dynamic equilibrium of intermediate adsorption–desorption. This further results in incomplete matching between theoretically predicted catalytic activity and experimental test results, restricting the accurate understanding of the catalytic essence.

To bridge the gap between theory and experiment, the construction of explicit solvation models and the introduction of constant potential conditions have become key breakthroughs in recent years. By explicitly incorporating solvent molecules and simulating real electrode potentials, such dynamic calculation models can reproduce the interfacial behavior and structural evolution under reaction scenarios. These results indicate that dynamic DFT models can provide more experiment-oriented theoretical guidance, offering reliable microscopic mechanism support for the structural design and performance enhancement of high-performance M-N-C catalysts.

In terms of experimental characterization, *in-situ* techniques have become the core means to capture the dynamic changes of catalysts during ORR. Among them, *in-situ* XAS, *in-situ* Raman spectroscopy, and *in-situ* infrared spectroscopy have been widely used due to their respective advantages. However, it should be noted that current *in-situ* characterization still has obvious shortcomings. First, the application of *in-situ* electron microscopy is relatively scarce. This technique can intuitively observe the macroscopic morphological changes of catalysts and the dynamic distribution of microactive sites during the reaction, but its strict requirements for the test environment limit its popularization; Second, existing characterizations mostly focus on single-dimensional information, making it difficult to simultaneously

Table 2 Summary of research breakthroughs in the combined use of dynamic DFT simulation and *in-situ* characterization techniques

Material type	Reaction type	Dynamic simulation	*In-situ* characterization	Breakthrough	Refs.
$FeCoN_6C$	ORR	Explicit solvation models Constant potential DFT pH dependence	*In-situ* SEIRAS spectra	Elucidating ORR activity regulation mechanisms under actual operating conditions.	[61]
NCMs	ORR	Constant potential DFT pH dependence	*In-situ* ATR-SEIRAS	Clarify the true active sites of NCMs under ORR conditions	[133]
FePc (Protic ionic liquid)	ORR	Explicit solvation models Constant potential DFT pH dependence	*In-situ* SEIRAS spectra	Clarify the pH-dependence of Protic ionic liquid under the ORR conditions.	[108]
$FePc/MoS_2$	ORR	Explicit solvation models	*In-situ* Raman spectra	Clarified the role of Lewis acid-base interactions in the oxygen reduction reaction	[131]
Electrolyte	ORR	Explicit solvation models pH dependence	*In-situ* NEXAFS *In-situ* Raman spectra	Clarified the role of alkali metal cations in the activity of ORR	[110]
Fe-Fe-N-C	ORR	Explicit solvation models	*In-situ* Raman spectra *In-situ* XAS	Revealing the active structure and reaction mechanism of the diatomic Fe site	[120]
$FeSnN_6C$	ORR	Explicit solvation models	*In-situ* FTIR *In-situ* XAS	Clarify the differences in ORR mechanisms between dual atom sites and single atom sites	[122]
Electrolyte	HER NRR	Ions effects Explicit Solvation models	*In-situ* FTIR spectra *In-situ* Raman spectra	The Faraday efficiency of NRR was 71% and the yield was 9.5×10^{-10} $mol \cdot s^{-1} \cdot cm^{-2}$ (with metal-free catalyst at −0.3 V vs. RHE).	[62]
$NiMoO_4$	HER	Ions effects Explicit solvation models	*In-situ* XAS	HER catalysts with stable operation over 1400 h at 0.45 $A \cdot cm^{-2}$	[59]

obtain the synergistic changes of geometric structure, electronic state, and intermediate behavior. It is necessary to realize comprehensive coverage of the dynamic changes in macroscopic/microscopic geometric structure and electronic structure of M-N-C catalysts during ORR through a series of *in-situ* characterizations combined with multiple techniques.

In general, the in-depth integration of dynamic DFT calculations and *in-situ* characterization techniques is the key path to breaking through the research bottlenecks of M-N-C catalysts. Dynamic DFT predicts the structure reconstruction, electronic state evolution, and thermodynamic trends induced by the real environment with atomic-level precision, providing microscopic mechanistic explanations for complex catalytic phenomena; *in-situ* characterization breaks through the limitations of traditional static characterization, real-time capturing dynamic changes under reaction conditions, and directly verifying the reliability of theoretical predictions. This synergistic model accurately analyzes the structure–performance correlation of M-N-C catalysts, providing solid scientific support for the design and development of new high-efficiency M-N-C catalysts.

6.2 Outlook

Although significant progress has been made in the theoretical and experimental research of M-N-C catalysts, there are still many challenges in the simulation of real reaction environments, cross-scale correlation, standardized evaluation, and theory-experiment in-depth coupling. Future research can focus on the following key directions to promote the field towards a more accurate, systematic, and application-oriented development:

(1) Optimize the balance between computational efficiency and accuracy in the simulation of real reaction environments. Although the use of explicit solvation models in the screening and design of new ORR catalysts such as M-N-C can enhance the authenticity of the simulation, the sharply increased number of solvent atoms raises the computational cost, further hindering the research and development cycle. In recent years, with the continuous development of static calculations, theoretical scientists have proposed many activity descriptors that have a good match with experimental activity. Therefore, in the future, when conducting research on new ORR materials using DFT, the advantages of activity descriptors in high-throughput material screening should be fully exploited. First, preliminary screening is carried out using activity volcanoes, d-band center theory and adsorption energy as descriptors to select materials with favorable intrinsic properties in static environments. These materials are then subjected to secondary screening and systematic research via dynamic DFT simulations that mimic practical reaction conditions.

(2) Utilizing machine learning (ML) to accelerate the study of dynamic interfaces. In recent years, ML, leveraging its advantages in data processing and performance prediction, has achieved significant success in developing new ORR catalysts in static environments. Therefore, similar workflow can be borrowed for dynamic ORR research. For dynamic DFT, many environmental factors such as pH value, voltage, types of ions in the solvent, etc. can be quantified as feature values, and then combined with the key feature values in static DFT calculations, such as the number of d-electrons of the active center metal, electronegativity, and the type of atoms at the active center, etc. Subsequently, a new database containing the static structure basis and dynamic environmental variables can be constructed to complete the screening and development of new catalysts. We also recognize that the construction of the dynamic environmental variable database is challenging and requires computational resources, but it is of great significance for the development and impact of new ORR materials, and can establish new research methods to push the development of ORR electrocatalysts into a new stage.

(3) Strengthen the deep coupling between dynamic density functional theory and *in-situ* characterization. In existing studies, theoretical calculations are based on idealized models and cannot reproduce the experimental scenarios of *in-situ* characterization. Meanwhile, the experimental characterization does not accurately design for the key dynamic processes predicted by the theory, resulting in a disconnection between the two. Based on this issue, first, theoretical researchers should deeply analyze the experimental conditions of *in-situ* characterization to conduct dynamic environment modeling, and try to replicate the real reaction environment rather than relying on their own experience judgments. Secondly, although *in-situ* characterization technology plays an important role in dynamic reaction research, its limitations should also be considered. For example, the signals generated by *in-situ* XAS are averages and are only sensitive to a limited number of substances. There are also problems such as spectral line overlap and field-induced frequency shift in *in-situ* Raman/infrared spectroscopy. Therefore, the study of dynamic ORR processes not only requires the establishment of a rigorous dynamic environment model, but also needs to consider the authenticity and reliability of *in-situ* characterization data.

Data availability

Not applicable.

Acknowledgements

This work was supported by the National Natural Science Foundation of China (No. 22508197), the Start-up Foundation offered by the Ningbo University of Technology (Nos. 2190011540029 and 2190011540014).

Declaration of competing interest

All the contributing authors report no conflict of interests in this work.

Author contribution statement

L. K. H.: Literatures collection, writing – original draft preparation, funding acquisition. J. M. L.: Data curation, writing – review & editing. Y. S.: Validation, writing – review & editing. H. D. Y.: Conceptualization, writing – review & editing. Y. H. L.: Data curation, writing – review & editing. X. D. L.: Validation, writing – review & editing. X. Q. W.: Conceptualization, writing – review & editing. J. M. L.: Administration, funding acquisition, writing – review & editing.

Use of AI statement

None.

References

[1] Müller-Hülstede, J.; Schmies, H.; Schonvogel, D.; Meyer, Q.; Nie,

Y.; Zhao, C.; Wagner, P.; Wark, M. What determines the stability of Fe–N–C catalysts in HT-PEMFCs. *Int. J. Hydrogen Energy* **2024**, *50*, 921–930.

[2] Ye, C. Z.; Zhang, L.; Shen, Y. Activity origin and catalytic mechanism of the M-N-C catalysts for the oxygen reduction reaction. *ACS Mater. Lett.* **2024**, *6*, 2858–2887.

[3] Huang, J. F.; Ajmal, S.; Kumar, A.; Guo, J. W.; Mujahid Alam, M.; Al-Sehemi, A. G.; Yasin, G. Atomically precise M-N-C electrocatalysts for oxygen reduction: Effects of inter-site distance, metal-metal interaction, coordination environment, and spin states. *J. Energy Chem.* **2025**, *101*, 132–155.

[4] Jin, Z. Y.; Chen, Y. Z.; Sun, J. L.; Zhang, S. M.; Zhang, J. J. Perceptions of metal-nitrogen-carbon catalysts for oxygen reduction reaction. *Mater. Sci. Eng.: R: Rep.* **2025**, *165*, 101027.

[5] Li, R. N.; Li, X. W.; Liu, Q. C.; Yue, H.; Meng, Y.; Tian, Y. Y. Effect of Fe–N–C single atom/cluster catalyst on ORR of PEMFC. *Int. J. Hydrogen Energy* **2025**, *139*, 718–729.

[6] Zhang, S. L.; Shi, M. X.; Wang, F. Y.; Lei, W.; Qiang, H.; Xia, M. Z. Research progress on non-precious-metal-based transition metal alkaline OER electrocatalysts. *J. Environ. Chem. Eng.* **2025**, *13*, 120378.

[7] Zhang, W. W.; Wang, Y.; Li, Y. C.; Sun, L. L.; Zhang, X. Y. First-principles calculations insight into non-noble-metal bifunctional electrocatalysts for zinc-air batteries. *Appl. Energy* **2025**, *391*, 125925.

[8] Chen, R.; Li, Y. F.; Liu, J. Q.; Hu, Z. C.; Hu, Q.; Fan, X. J. Design, mechanisms, and applications of iron-based metal-organic frameworks derived electrocatalysts for zinc-air batteries. *J. Energy Storage* **2026**, *142*, 119482.

[9] Kumar, A.; Goyal, N.; Mathur, S.; Bakhtiyarovich, I. A.; Zhao, Y. F.; Khalid, M.; Ubaidullah, M.; Al-Enizi, A. M. Advances in coordination engineering of M-N-C single atom catalysts for superior oxygen reduction performance. *Coord. Chem. Rev.* **2026**, *549*, 217244.

[10] Lyu, C. J.; Yang, J. X.; Guo, H. Y.; Cheng, J. R.; Geng, D. S.; Liu, Y. M. Co-based bifunctional OER/ORR electrocatalysts: From nanostructure engineering to catalytic mechanism innovation for cutting-edge research in empowering energy conversion systems. *Coord. Chem. Rev.* **2026**, *551*, 217393.

[11] Xie, X. H.; He, C.; Li, B. Y.; He, Y. H.; Cullen, D. A.; Wegener, E. C.; Kropf, A. J.; Martinez, U.; Cheng, Y. W.; Engelhard, M. H. et al. Performance enhancement and degradation mechanism identification of a single-atom Co-N-C catalyst for proton exchange membrane fuel cells. *Nat. Catal.* **2020**, *3*, 1044–1054.

[12] Mi, C. X.; Yu, H. F.; Han, L. K.; Zhang, L. R.; Zhai, L. L.; Li, X. L.; Liu, Y. J.; Xiang, Z. H. Symmetric electronic structures of active sites to boost bifunctional oxygen electrocatalysis by MN_{4+4} sites directly from initial covalent organic polymers. *Adv. Funct. Mater.* **2023**, *33*, 2303235.

[13] Niu, Z. Q.; Lu, Z. K.; Qiao, Z. L.; Xing, M. H.; Han, L. K.; Wang, S. T.; Cao, D. P. Long-range regulation of Se doping for oxygen reduction of atomically dispersed sb catalysts for ultralow-temperature solid-state Zn-air batteries. *ACS Catal.* **2023**, *13*, 7122–7131.

[14] Luo, M. Y.; Cai, X. Y.; Ni, Y. X.; Chen, Y. Z.; Guo, C. S.; Wang, H. Y. From porphyrin-like rings to high-density single-atom catalytic sites: Unveiling the superiority of p-C_2N for bifunctional oxygen electrocatalysis. *ACS Appl. Mater. Interfaces* **2024**, *16*, 807–818.

[15] Guo, M. M.; Ji, M.; Cui, W. Theoretical investigation of HER/OER/ORR catalytic activity of single atom-decorated graphyne by DFT and comparative DOS analyses. *Appl. Surf. Sci.* **2022**, *592*, 153237.

[16] Liu, J. L.; Xiao, J. X.; Luo, B. C.; Tian, E. K.; Waterhouse, G. I. N. Central metal and ligand effects on oxygen electrocatalysis over 3D transition metal single-atom catalysts: A theoretical investigation. *Chem. Eng. J.* **2022**, *427*, 132038.

[17] Li, X. Y.; Su, Z. H.; Zhao, Z. F.; Cai, Q. H.; Li, Y. F.; Zhao, J. X. Single Ir atom anchored in pyrrolic-N_4 doped graphene as a promising bifunctional electrocatalyst for the ORR/OER: A computational study. *J. Colloid Interface Sci.* **2022**, *607*, 1005–1013.

[18] He, L. H.; Li, T.; Hu, H.; Xie, P. F.; Li, J. C. Understanding the three-shell coordination structure-performance relationship of single-atom sites for oxygen reduction using molecular model catalysts. *ACS Catal.* **2025**, *15*, 13391–13400.

[19] Yang, J.; Liu, W. G.; Xu, M. Q.; Liu, X. Y.; Qi, H. F.; Zhang, L. L.; Yang, X. F.; Niu, S. S.; Zhou, D.; Liu, Y. F. et al. Dynamic behavior of single-atom catalysts in electrocatalysis: Identification of Cu-N_3 as an active site for the oxygen reduction reaction. *J. Am. Chem. Soc.* **2021**, *143*, 14530–14539.

[20] Wei, J.; Xia, D. S.; Wei, Y. P.; Zhu, X. Y.; Li, J.; Gan, L. Probing the oxygen reduction reaction intermediates and dynamic active site structures of molecular and pyrolyzed Fe-N-C electrocatalysts by *in situ* Raman spectroscopy. *ACS Catal.* **2022**, *12*, 7811–7820.

[21] Liu, H.; Zhang, D.; Wang, Y.; Li, H. Reversible hydrogen electrode (RHE) scale dependent surface Pourbaix diagram at different pH. *Langmuir* **2024**, *40*, 7632–7638.

[22] Lu, F. H.; Zhang, Y. Y.; Zong, L. B.; Wang, C. B.; Fan, K. C.; Chuang, C. H.; Liu, P. R.; Wang, Z. M.; Wang, L.; Li, B. Fe, P heteronuclear catalytic pairs with hydrogen bonding regulated the oxygen reduction reaction kinetics for an ultrastable oxygen depolarized cathode. *ACS Nano* **2025**, *19*, 40128–40139.

[23] Abidin, A. F. Z.; Hamada, I. Oxygen reduction reaction on single-atom catalysts from density functional theory calculations combined with an implicit solvation model. *J. Phys. Chem. C* **2023**, *127*, 13623–13631.

[24] Xiao, M. L.; Chen, Y. T.; Zhu, J. B.; Zhang, H.; Zhao, X.; Gao, L. Q.; Wang, X.; Zhao, J.; Ge, J. J.; Jiang, Z. et al. Climbing the apex of the ORR volcano plot via binuclear site construction: Electronic and geometric engineering. *J. Am. Chem. Soc.* **2019**, *141*, 17763–17770.

[25] Qin, Y. Y.; Li, P.; Li, Z.; Wu, T. T.; Su, Y. Q. Potential-dependent oxygen reduction on FeN_4 under explicit solvation environment. *J. Phys. Chem. C* **2023**, *127*, 4934–4941.

[26] Cai, Z. F.; Wang, X.; Wang, D.; Wan, L. J. Cobalt-porphyrin-catalyzed oxygen reduction reaction: A scanning tunneling microscopy study. *ChemElectroChem* **2016**, *3*, 2048–2051.

[27] Han, L. K.; Qiu, W. H.; Xiang, Z. H. An environmental corrected descriptor based on *d*-orbital spin states for atomically dispersed dual-metal catalysts. *AlChE J.* **2024**, *70*, e18459.

[28] Han, L. K.; Yu, H. F.; Xiang, Z. H. Asymmetric active sites for boosting oxygen evolution reaction. *Small* **2023**, *19*, 2304108.

[29] Noh, J.; Kim, H.; Park, H.; Chung, D. Y. The roles of ions in electrochemical interface for electrocatalysis. *ACS Catal.* **2025**, *15*, 7780–7791.

[30] Yan, H. M.; Wang, G.; Lv, X. M.; Cao, H.; Qin, G. Q.; Wang, Y. G. Revealing the potential-dependent rate-determining step of oxygen reduction reaction on single-atom catalysts. *J. Am. Chem. Soc.* **2025**, *147*, 3724–3730.

[31] Carrasco, J.; Klimeš, J.; Michaelides, A. The role of van der Waals forces in water adsorption on metals. *J. Chem. Phys.* **2013**, *138*, 024708.

[32] Di Liberto, G.; Giordano, L. Role of solvation model on the stability of oxygenates on Pt(111): A comparison between microsolvation, extended bilayer, and extended metal/water interface. *Electrochem. Sci. Adv.* **2024**, *4*, e2100204.

[33] Chun, H. J.; Morankar, A.; Zeng, Z. H.; Greeley, J. Solvation enthalpy determination for aqueous-phase reaction adsorbates using *ab initio* molecular dynamics-based structure sampling. *J. Phys. Chem. C* **2024**, *128*, 1621–1632.

[34] Chan, K.; Nørskov, J. K. Potential dependence of electrochemical barriers from *ab initio* calculations. *J. Phys. Chem. Lett.* **2016**, *7*, 1686–1690.

[35] Yu, S.; Levell, Z.; Jiang, Z.; Zhao, X. H.; Liu, Y. Y. What is the rate-limiting step of oxygen reduction reaction on Fe-N-C catalysts. *J. Am. Chem. Soc.* **2023**, *145*, 25352–25356.
[36] Zhang, D.; Wang, Z. Y.; Liu, F. Z.; Yi, P. Y.; Peng, L. F.; Chen, Y.; Wei, L.; Li, H. Unraveling the pH-dependent oxygen reduction performance on single-atom catalysts: From single- to dual-sabatier optima. *J. Am. Chem. Soc.* **2024**, *146*, 3210–3219.
[37] Ye, S. B.; Wang, Y. H.; Liu, H.; Zhang, D.; Jia, X.; Zhang, L. D.; Zhang, Y. Z.; Kumatani, A.; Shiku, H.; Li, H. Decoding pH-dependent electrocatalysis through electric field models and microkinetic volcanoes. *J. Mater. Chem. A* **2025**, *13*, 37821–37832.
[38] Magnussen, O. M.; Groß, A. Toward an atomic-scale understanding of electrochemical interface structure and dynamics. *J. Am. Chem. Soc.* **2019**, *141*, 4777–4790.
[39] Swift, M. W.; Swift, J. W.; Qi, Y. Modeling the electrical double layer at solid-state electrochemical interfaces. *Nat. Comput. Sci.* **2021**, *1*, 212–220.
[40] Mathew, K.; Kolluru, V. S. C.; Mula, S.; Steinmann, S. N.; Hennig, R. G. Implicit self-consistent electrolyte model in plane-wave density-functional theory. *J. Chem. Phys.* **2019**, *151*, 234101.
[41] Nørskov, J. K.; Rossmeisl, J.; Logadottir, A.; Lindqvist, L.; Kitchin, J. R.; Bligaard, T.; Jónsson, H. Origin of the overpotential for oxygen reduction at a fuel-cell cathode. *J. Phys. Chem. B* **2004**, *108*, 17886–17892.
[42] Low, J. L.; Roth, C.; Paulus, B. exploring the inner- and outer-sphere mechanistic pathways of ORR on M-N-Cs with pyrrolic MN_4 motifs. *J. Phys. Chem. C* **2024**, *128*, 5075–5083.
[43] Rossmeisl, J.; Logadottir, A.; Nørskov, J. K. Electrolysis of water on (oxidized) metal surfaces. *Chem. Phys.* **2005**, *319*, 178–184.
[44] Ringe, S.; Hörmann, N. G.; Oberhofer, H.; Reuter, K. Implicit solvation methods for catalysis at electrified interfaces. *Chem. Rev.* **2022**, *122*, 10777–10820.
[45] Groß, A. Grand-canonical approaches to understand structures and processes at electrochemical interfaces from an atomistic perspective. *Curr. Opin. Electrochem.* **2021**, *27*, 100684.
[46] Xia, D. S.; Yu, C. C.; Zhao, Y. H.; Wei, Y. P.; Wu, H. Y.; Kang, Y. Q.; Li, J.; Gan, L.; Kang, F. Y. Degradation and regeneration of Fe–N_x active sites for the oxygen reduction reaction: The role of surface oxidation, Fe demetallation and local carbon microporosity. *Chem. Sci.* **2021**, *12*, 11576–11584.
[47] Zhang, Z. S.; Li, J.; Wang, Y. G. Modeling interfacial dynamics on single atom electrocatalysts: Explicit solvation and potential dependence. *Acc. Chem. Res.* **2024**, *57*, 198–207.
[48] Li, H.; Luan, D.; Long, J.; Guo, P.; Xiao, J. P. Electrochemical reaction kinetics at constant interfacial potential. *ACS Catal.* **2024**, *14*, 12814–12823.
[49] Yeh, K. Y.; Janik, M. J. Density functional theory-based electrochemical models for the oxygen reduction reaction: Comparison of modeling approaches for electric field and solvent effects. *J. Comput. Chem.* **2011**, *32*, 3399–3408.
[50] Nair, A. S.; Pathak, B. Accounting for dispersion effects in the DFT framework of electrocatalysis: A hybrid solvation model-based case study of the oxygen reduction reaction. *J. Phys. Chem. C* **2022**, *126*, 6171–6188.
[51] Ezhov, R.; Maximova, O.; Lyu, X.; Leshchev, D.; Stavitski, E.; Serov, A.; Pushkar, Y. Spectroscopic characterization of highly active Fe–N–C oxygen reduction catalysts and discovery of strong interaction with nafion ionomer. *ACS Appl. Energy Mater.* **2024**, *7*, 604–613.
[52] Wu, B.; Sun, T. X.; You, Y.; Meng, H. B.; Morales, D. M.; Lounasvuori, M.; Beheshti Askari, A.; Jiang, L.; Zeng, F.; Hu, B. S. et al. *In situ* X-ray absorption spectroscopy of metal/nitrogen-doped carbons in oxygen electrocatalysis. *Angew. Chem., Int. Ed.* **2023**, *62*, e202219188.
[53] Alsudairi, A.; Li, J. K.; Ramaswamy, N.; Mukerjee, S.; Abraham, K. M.; Jia, Q. Y. Resolving the iron phthalocyanine redox transitions for ORR catalysis in aqueous media. *J. Phys. Chem. Lett.* **2017**, *8*, 2881–2886.
[54] Wan, L. Y.; Zhao, K. M.; Wang, Y. C.; Wei, N.; Zhang, P. Y.; Yuan, J. Y.; Zhou, Z. Y.; Sun, S. G. Molecular degradation of iron phthalocyanine during the oxygen reduction reaction in acidic media. *ACS Catal.* **2022**, *12*, 11097–11107.
[55] Song, J. T.; Qian, Z. X.; Yang, J.; Lin, X. M.; Xu, Q. C.; Li, J. F. *In situ*/operando investigation for heterogeneous electro-catalysts: From model catalysts to state-of-the-art catalysts. *ACS Energy Lett.* **2024**, *9*, 4414–4440.
[56] Ding, J.; Liu, L. Y.; Zhang, J.; Liu, Y. H.; Xu, H.; Shen, Z.; Yang, H. B.; Feng, X. L.; Huang, Y. Q.; Liu, B. Unraveling dynamic structural evolution of single atom catalyst via *in situ* surface-enhanced infrared absorption spectroscopy. *J. Am. Chem. Soc.* **2025**, *147*, 9601–9609.
[57] Gu, J. Y.; Cai, Z. F.; Wang, D.; Wan, L. J. Single-molecule imaging of iron-phthalocyanine-catalyzed oxygen reduction reaction by *in situ* scanning tunneling microscopy. *ACS Nano* **2016**, *10*, 8746–8750.
[58] Zhao, Y. G.; Adiyeri Saseendran, D. P.; Huang, C.; Triana, C. A.; Marks, W. R.; Chen, H.; Zhao, H.; Patzke, G. R. Oxygen evolution/reduction reaction catalysts: From *in situ* monitoring and reaction mechanisms to rational design. *Chem. Rev.* **2023**, *123*, 6257–6358.
[59] Chang, B.; Liu, X. Y.; Zuo, S. W.; Ren, Y. F.; He, J. T.; Wang, D. Q.; Lei, Y. J.; Hu, M.; Li, W. L.; Khan, M. A. et al. Dynamic construction of a durable epitaxial catalytic layer for industrial alkaline water splitting. *Nat. Commun.* **2025**, *16*, 7959.
[60] Li, P.; Jiang, Y. L.; Men, Y.; Jiao, Y. Z.; Chen, S. L. Kinetic cation effect in alkaline hydrogen electrocatalysis and double layer proton transfer. *Nat. Commun.* **2025**, *16*, 1844.
[61] Li, P.; Jiao, Y. Z.; Ruan, Y. E.; Fei, H. G.; Men, Y.; Guo, C. L.; Wu, Y. E.; Chen, S. L. Revealing the role of double-layer microenvironments in pH-dependent oxygen reduction activity over metal-nitrogen-carbon catalysts. *Nat. Commun.* **2023**, *14*, 6936.
[62] Wang, M. F.; Liu, S. S.; Ji, H. Q.; Yang, T. Z.; Qian, T.; Yan, C. L. Salting-out effect promoting highly efficient ambient ammonia synthesis. *Nat. Commun.* **2021**, *12*, 3198.
[63] Zhao, Y. S.; Wan, J. W.; Ling, C. Y.; Wang, Y. L.; He, H. Y.; Yang, N. L.; Wen, R.; Zhang, Q. H.; Gu, L.; Yang, B. L. et al. Acidic oxygen reduction by single-atom Fe catalysts on curved supports. *Nature* **2025**, *644*, 668–675.
[64] Yu, H. F.; Li, C. C.; Lei, Y. Y.; Xiang, Z. H. Strategic secondary coordination implantation towards efficient and stable Fe–N–C electrocatalysts for the oxygen reduction reaction in PEMFCs. *Angew. Chem., Int. Ed.* **2025**, *64*, e202508141.
[65] Qi, Y. G.; Song, K. X.; Liang, Q.; Zhou, X. Y.; Liu, M. Q.; Li, W. W.; Liu, F. X.; Jiang, Z.; Gu, Q. H.; Chen, Z. J. et al. Asymmetric B-coordination stimulated high-spin cobalt boosts ORR. *Nano Res.* **2025**, *18*, 94907278.
[66] Kulkarni, A.; Siahrostami, S.; Patel, A.; Nørskov, J. K. Understanding catalytic activity trends in the oxygen reduction reaction. *Chem. Rev.* **2018**, *118*, 2302–2312.
[67] Shao, M. H.; Chang, Q. W.; Dodelet, J. P.; Chenitz, R. Recent advances in electrocatalysts for oxygen reduction reaction. *Chem. Rev.* **2016**, *116*, 3594–3657.
[68] Jasinski, R. A new fuel cell cathode catalyst. *Nature* **1964**, *201*, 1212–1213.
[69] Lefèvre, M.; Proietti, E.; Jaouen, F.; Dodelet, J. P. Iron-based catalysts with improved oxygen reduction activity in polymer electrolyte fuel cells. *Science* **2009**, *324*, 71–74.
[70] Li, X. L.; Xiang, Z. H. Identifying the impact of the covalent-bonded carbon matrix to FeN_4 sites for acidic oxygen reduction. *Nat. Commun.* **2022**, *13*, 57.
[71] Zitolo, A.; Goellner, V.; Armel, V.; Sougrati, M. T.; Mineva, T.; Stievano, L.; Fonda, E.; Jaouen, F. Identification of catalytic sites for

oxygen reduction in iron- and nitrogen-doped graphene materials. *Nat. Mater.* **2015**, *14*, 937–942.

[72] Li, S. L.; Shi, L.; Guo, Y. J.; Wang, J. Y.; Liu, D.; Zhao, S. L. Selective oxygen reduction reaction: Mechanism understanding, catalyst design and practical application. *Chem. Sci.* **2024**, *15*, 11188–11228.

[73] Chen, Y. J.; Ji, S. F.; Chen, C.; Peng, Q.; Wang, D. S.; Li, Y. D. Single-atom catalysts: Synthetic strategies and electrochemical applications. *Joule* **2018**, *2*, 1242–1264.

[74] He, Y. T.; Yang, X. X.; Li, Y. S.; Liu, L. T.; Guo, S. W.; Shu, C. Y.; Liu, F.; Liu, Y. N.; Tan, Q.; Wu, G. Atomically dispersed Fe–Co dual metal sites as bifunctional oxygen electrocatalysts for rechargeable and flexible Zn-air batteries. *ACS Catal.* **2022**, *12*, 1216–1227.

[75] Tang, B.; Ji, Q. Q.; Zhang, X. L.; Shi, R. C.; Ma, J.; Zhuang, Z. C.; Sun, M.; Wang, H. J.; Liu, R. Q.; Liu, H. J. et al. Symmetry breaking of FeN_4 moiety via edge defects for acidic oxygen reduction reaction. *Angew. Chem., Int. Ed.* **2025**, *64*, e202424135.

[76] Yang, B. L.; Han, L. K.; Shen, Y. F.; Peng, J. F.; Liu, W. Q.; Gu, T.; Wu, Z. S. Tuning the coordination field configuration on well-defined molecular catalysts for boosting bifunctional oxygen electrocatalytic. *Chem. Eng. J.* **2026**, *529*, 172845.

[77] Menga, D.; Li, Y. S.; Damjanović, A. M.; Proux, O.; Wagner, F. E.; Fellinger, T. P.; Gasteiger, H. A.; Piana, M. On the stability of an atomically-dispersed Fe-N-C ORR catalyst: An *in situ* XAS study in a PEMFC. *ChemElectroChem* **2024**, *11*, e202400228.

[78] Liu, J. C.; Xiao, H.; Zhao, X. K.; Zhang, N. N.; Liu, Y.; Xing, D. H.; Yu, X. H.; Hu, H. S.; Li, J. Computational prediction of graphdiyne-supported three-atom single-cluster catalysts. *CCS Chem.* **2023**, *5*, 152–163.

[79] Jiang, R.; Qiao, Z. L.; Xu, H. X.; Cao, D. P. Defect engineering of Fe–N–C single-atom catalysts for oxygen reduction reaction. *Chin. J. Catal.* **2023**, *48*, 224–234.

[80] Liu, G. D.; Deng, H. Q.; Greeley, J.; Zeng, Z. H. Density functional theory study of active sites and reaction mechanism of ORR on Pt surfaces under anhydrous conditions. *Chin. J. Catal.* **2022**, *43*, 3126–3133.

[81] Yu, Z. P.; Si, C. W.; LaGrow, A. P.; Tai, Z. X.; Caliebe, W. A.; Tayal, A.; Sampaio, M. J.; Sousa, J. P. S.; Amorim, I.; Araujo, A. et al. Iridium-iron diatomic active sites for efficient bifunctional oxygen electrocatalysis. *ACS Catal.* **2022**, *12*, 9397–9409.

[82] Han, X. P.; Ling, X. F.; Yu, D. S.; Xie, D. Y.; Li, L. L.; Peng, S. J.; Zhong, C.; Zhao, N. Q.; Deng, Y. D.; Hu, W. B. Atomically dispersed binary Co–Ni sites in nitrogen-doped hollow carbon nanocubes for reversible oxygen reduction and evolution. *Adv. Mater.* **2019**, *31*, 1905622.

[83] Wang, J.; Huang, Z. Q.; Liu, W.; Chang, C. R.; Tang, H. L.; Li, Z. J.; Chen, W. X.; Jia, C. J.; Yao, T.; Wei, S. Q. et al. Design of N-coordinated dual-metal sites: A stable and active Pt-free catalyst for acidic oxygen reduction reaction. *J. Am. Chem. Soc.* **2017**, *139*, 17281–17284.

[84] Kumar, A.; Ubaidullah, M.; Yasin, G. Investigating the effect of active site's coordination number on the oxygen reduction reaction activity of Fe–Co dual-atom catalysts: A theoretical study. *Int. J. Hydrogen Energy* **2025**, *109*, 694–702.

[85] Yu, K.; Qin, J.; Zhang, H.; Zhang, S. L.; Cao, Y. Y.; Xie, C.; Yang, H. J.; Xiao, W.; Li, W. B.; Zhang, G. N. et al. Tailoring the first/second coordination layer of FeNi single atoms with nucleophile atoms to boost oxygen electrocatalysis for zinc-air batteries. *Adv. Funct. Mater.* **2025**, *15*, 2501091.

[86] Chen, L. Z.; Wang, X.; Lu, T. Y.; Pang, H.; Zhang, S. T.; Xu, L.; Yang, G. X.; Zhou, Q. X.; Tang, Y. W. Maneuver of the d-orbital spin polarization of Fe single atomic sites via a near-range axial ligand effect for boosting oxygen reduction reaction. *App. Catal. B: Environ. Energy* **2025**, *366*, 125007.

[87] Mou, Y. M.; Gao, S. R.; Wang, Y.; Li, Y. F. Axial coordination engineering on Fe-N-C materials for oxygen reduction: Insights from theory. *Chem. Eur. J.* **2024**, *30*, e202402869.

[88] Zhang, Z.; Yang, L.; Liu, J. R.; Hu, H.; Mi, J. L.; Su, C.; Xiao, B. B.; Ao, Z. M. Improved oxygen electrocatalysis at FeN_4 and CoN_4 sites via construction of axial coordination. *Chin. Chem. Lett.* **2025**, *36*, 110013.

[89] Zhang, S. Y.; Sun, B. W.; Liao, K.; Wang, X.; Chen, Z. Y.; Wang, J. J.; Hu, W. B.; Han, X. P. Boosting oxygen reduction reaction performance of Fe single-atom catalysts via precise control of the coordination environment. *Adv. Funct. Mater.* **2025**, *35*, 2425640.

[90] Cao, Y. H.; Liu, Y.; Zheng, X. R.; Yang, J. X.; Wang, H. Z.; Zhang, J. F.; Han, X. P.; Deng, Y. D.; Rupprechter, G.; Hu, W. B. Quantifying asymmetric coordination to correlate with oxygen reduction activity in Fe-based single-atom catalysts. *Angew. Chem., Int. Ed.* **2025**, *64*, e202423556.

[91] Xu, X. Q.; Gan, T.; Guan, J. Q. Spin engineering of dual-atom Fe_2 catalysts for oxygen reduction. *CCS Chem.* **2026**, *8*, 350–367.

[92] Li, D. Y.; Xu, H. X.; Zhu, J. Q.; Cao, D. P. Fast identification of the stability of atomically dispersed bi-atom catalysts using a structure descriptor-based model. *J. Mater. Chem. A* **2022**, *10*, 1451–1462.

[93] Xu, H. X.; Cheng, D. J.; Cao, D. P.; Zeng, X. C. RETRACTED ARTICLE: A universal principle for a rational design of single-atom electrocatalysts. *Nat. Catal.* **2018**, *1*, 339–348.

[94] Armillotta, F.; Bidoggia, D.; Baronio, S.; Biasin, P.; Annese, A.; Scardamaglia, M.; Zhu, S. Y.; Bozzini, B.; Modesti, S.; Peressi, M. et al. Single metal atom catalysts and ORR: H-bonding, solvation, and the elusive hydroperoxyl intermediate. *ACS Catal.* **2022**, *12*, 7950–7959.

[95] Yang, X. C.; Peng, C.; Hou, M. J.; Zhang, D.; Yang, B.; Xue, D. F.; Lei, Y.; Liang, F. Rational design of electrolyte solvation structures for modulating $2e^-/4e^-$ transfer in sodium-air batteries. *Adv. Funct. Mater.* **2022**, *32*, 2201258.

[96] Melander, M. M.; Kuisma, M. J.; Christensen, T. E. K.; Honkala, K. Grand-canonical approach to density functional theory of electrocatalytic systems: Thermodynamics of solid–liquid interfaces at constant ion and electrode potentials. *J. Chem. Phys.* **2019**, *150*, 041706.

[97] Zhang, D.; Li, H. The potential of zero charge and solvation effects on single-atom M-N-C catalysts for oxygen electrocatalysis. *J. Mater. Chem. A* **2024**, *12*, 13742–13750.

[98] Andreussi, O.; Dabo, I.; Marzari, N. Revised self-consistent continuum solvation in electronic-structure calculations. *J. Chem. Phys.* **2012**, *136*, 064102.

[99] Kirchhoff, B.; Jónsson, E. Ö.; Jacob, T.; Jónsson, H. On the challenge of obtaining an accurate solvation energy estimate in simulations of electrocatalysis. *Top. Catal.* **2023**, *66*, 1244–1259.

[100] Deng, C. F.; Deng, C.; Hu, S. W.; Ren, Y. R. Mechanistic insights into the oxygen reduction reaction on the Fe-N_4/C single-atom catalysts: Spectator species and solvent as the key driving force. *Surf. Sci.* **2026**, *765*, 122875.

[101] Wang, Y. M.; Yan, H. M.; Cao, H.; Chen, J. W.; Yang, H.; Zhu, J. Y.; Sun, J. Atomic-scale understanding of electrified interfacial structures and dynamics during the oxygen reduction reaction on the Fe–N_4/C electrocatalyst. *ACS Catal.* **2023**, *13*, 11080–11090.

[102] Ren, P. H.; Feng, Z. B.; Zhao, Y.; Liu, C. Y.; Li, H. X.; Li, R. P.; Chen, X. B. Exploring the impact of S-doped Fe–N–C materials on the ORR mechanism within a constant potential solvation model. *Mol. Catal.* **2024**, *559*, 114119.

[103] Morankar, A.; Deshpande, S.; Zeng, Z. H.; Atanassov, P.; Greeley, J. A first principles analysis of potential-dependent structural evolution of active sites in Fe-N-C catalysts. *Proc. Natl. Acad. Sci. USA* **2023**, *120*, e2308458120.

[104] Tamtaji, M.; Li, Y. Y.; Cai, Y. T.; Liu, H. W.; Goddard III, W. A.; Chen, G. H. Reaction mechanism and kinetics of oxygen reduction reaction on the iron-nickel dual atom catalyst. *J. Mater. Chem. A* **2023**, *11*, 25410–25421.

[105] Resasco, J. A universal model of cation effects in electrocatalysis. *JACS Au* **2025**, *5*, 5253–5266.
[106] Chen, S. L.; Yu, Q. H.; Ji, Y. J.; Li, Y. Y. Unveiling electrolyte effects on the oxygen reduction at Co-N-C single-atom catalysts in nonaqueous lithium-oxygen batteries by *ab initio* molecular dynamics. *ACS Catal.* **2025**, *15*, 16782–16791.
[107] Li, Y.; Chen, M. Y.; Lu, B. A.; Wu, H. R.; Zhang, J. N. Unravelling the role of hydrogen peroxide in pH-dependent ORR performance of Mn-N-C catalysts. *App. Catal. B: Environ.* **2024**, *342*, 123458.
[108] Men, Y.; Jiao, Y. Z.; Zheng, Y. X.; Wang, X. Y.; Chen, S. L.; Li, P. pH-dependent protic ionic liquid tuning effect on oxygen reduction activity of a molecular iron catalyst and its electrochemical interfacial origin. *Chin. J. Catal.* **2026**, *80*, 258–269.
[109] Tian, Y. M.; Hou, P. F.; Zhou, Y. Y.; Li, Q. Alkali metal cations induce pseudo-outer-sphere oxygen reduction reaction mechanism in electrolyte-catalyst synergy. *J. Am. Chem. Soc.* **2025**, *147*, 35118–35127.
[110] Ji, S. G.; Kim, M. M.; Han, M. H.; Cho, J.; Son, Y.; Kim, Y. Y.; Jeong, J.; Kim, Z. H.; Chae, K. H.; Oh, H. S. et al. Alkali metal cations act as homogeneous cocatalysts for the oxygen reduction reaction in aqueous electrolytes. *Nat. Catal.* **2024**, *7*, 1330–1338.
[111] Zhao, Y. L.; Ji, Z.; Xiao, X.; Fang, Z.; Hou, Y. L. Decoupling of spin and non-spin effects from electronic structure modulation for oxygen electrocatalysis. *Adv. Sci.* **2025**, *12*, e14540.
[112] Jung, H.; Fanta, R.; Hossain, M. D.; Bajdich, M. Spin state modulation in M-N-C single-atom catalysts for oxygen electrocatalysis. *ACS Catal.* **2025**, *15*, 16380–16387.
[113] Zheng, T.; Wang, J. C.; Xia, Z. H.; Wang, G. F.; Duan, Z. Y. Spin-dependent active centers in Fe–N–C oxygen reduction catalysts revealed by constant-potential density functional theory. *J. Mater. Chem. A* **2023**, *11*, 19360–19373.
[114] Cheng, R. Q.; He, X. Q.; Jiang, M.; Shao, X. C.; Tang, W. Q.; Ran, B.; Li, H. X.; Fu, C. P. f-p-d gradient orbital coupling induced spin state enhancement of atomic Fe sites for efficient and stable oxygen reduction reaction. *Adv. Funct. Mater.* **2025**, *35*, 2425138.
[115] Mei, Z. Y.; Zhao, G. F.; Xia, C. F.; Cai, S.; Jing, Q.; Sheng, X. L.; Wang, H.; Zou, X. X.; Wang, L. L.; Guo, H. et al. Regulated high-spin state and constrained charge behavior of active cobalt sites in covalent organic frameworks for promoting electrocatalytic oxygen reduction. *Angew. Chem., Int. Ed.* **2023**, *62*, e202303871.
[116] Wang, L. L.; Mei, Z. Y.; An, Q.; Sheng, X. L.; Jing, Q.; Huang, W. J.; Wang, X. F.; Zou, X. X.; Guo, H. Modulating the electronic spin state of atomically dispersed iron sites by adjacent zinc atoms for enhanced spin-dependent oxygen electrocatalysis. *Chem. Catal.* **2023**, *3*, 100758.
[117] Yu, M. Y.; Li, A.; Kan, E. J.; Zhan, C. Substantial impact of spin state evolution in OER/ORR catalyzed by Fe-N-C. *ACS Catal.* **2024**, *14*, 6816–6826.
[118] Zhao, Z. X.; Yu, M. Y.; Kan, E. J.; Zhan, C. Spin-dominated oxygen activation and reduction mechanism on a Ru-N-C single-atom-catalyst. *Phys. Chem. Chem. Phys.* **2025**, *27*, 24827–24834.
[119] Song, K. X.; Yang, B. B.; An, W. G.; Liang, Q.; Lin, J. K.; Zhang, H. Y.; Qi, Y. G.; Lai, Y. C.; Chen, Z. J.; Li, W. W. et al. Dynamic spin governing asymmetric coordination fields in trimetallic single-atom catalysts for optimal oxygen reduction. *Angew. Chem., Int. Ed.*, in press, https://doi.org/10.1002/ange.202519740.
[120] Li, R.; Sun, X. X.; Yang, L.; Zhao, P. P.; Zhao, J. G.; Ding, J.; Wu, S. L.; Li, C. G.; Liu, H.; Dong, S. J. Deciphering the effect of interfacial dipole between dinuclear Fe sites and oxygen on breaking activity-stability trade-off in acidic oxygen reduction reaction. *App. Catal. B: Environ. Energy* **2026**, *383*, 126065.
[121] Chang, S. T.; Liu, H. X.; Chu, Y. C.; Lu, Y. R.; Wang, C. H. Revealing the *operando* ORR mechanism of single-atom catalysts anchored in nanobowl structures for advanced hydroxide exchange membrane fuel cells. *Chem. Eng. J.* **2026**, *528*, 172462.
[122] Zhang, C.; Guo, Y. S.; Chen, C.; Zhuang, Z. W.; You, S. P.; Yu, M. Y.; Tan, X.; Sun, K. A.; Peng, Q.; Yan, W. et al. Accelerated O–O bond cleavage and stabilized Fe sites by synergistic d-p Fe–Sn dual-atom pair for enhanced oxygen reduction. *Angew. Chem., Int. Ed.* **2026**, *65*, e24265.
[123] Yuan, L. J.; Miao, Z. Y.; Sui, X. L.; Lee, C. F.; Li, Q.; Yin, M. J.; Shen, L. X.; Lu, Y. R.; Zhao, Z. G.; Liu, Y. Z. et al. Janus effect of FeCo dual atom catalyst with Co as active center in acidic oxygen reduction reaction. *Nat. Comm.* **2025**, *16*, 7198.
[124] Sui, R.; Liu, B.; Chen, C.; Tan, X.; He, C.; Xin, D. Y.; Chen, B. W.; Xu, Z. Y.; Li, J. Z.; Chen, W. X. et al. Constructing asymmetric Fe–Nb diatomic sites to enhance ORR activity and durability. *J. Am. Chem. Soc.* **2024**, *146*, 26442–26453.
[125] Xu, W. X.; Zeng, R.; Rebarchik, M.; Posada-Borbón, A.; Li, H. Q.; Pollock, C. J.; Mavrikakis, M.; Abruña, H. D. Atomically dispersed Zn/Co–N–C as ORR electrocatalysts for alkaline fuel cells. *J. Am. Chem. Soc.* **2024**, *146*, 2593–2603.
[126] Wang, F. B.; He, X. Y.; Qu, G. M.; Mamoor, M.; Zhai, Y. J.; Wang, L.; Wang, B.; Jing, Z. X.; Kong, Y. Y.; Wang, D. D. et al. Coupling optimized Fe–N coordination structure-dominant cathode with *in situ* hydrogel electrolytes toward a highly efficient flexible Zn-air battery. *ACS Nano* **2025**, *19*, 22330–22342.
[127] Bhardwaj, S.; Pathak, A.; Das, S. K.; Das, P.; Thapa, R.; Dey, R. S. Decoding dual-functionality in N-doped defective carbon: Unveiling active sites for bifunctional oxygen electrocatalysis. *Small* **2025**, *21*, 2411035.
[128] Zhang, X. H.; Zhang, X. R.; Li, X. X.; Han, G. Y.; Zhu, S.; Li, Y. Curvature-induced oxygen reduction activity regulation of asymmetric CoN_2O_2 catalytic sites in covalent organic polymers. *App. Catal. B: Environ. Energy* **2026**, *385*, 126330.
[129] Friesen, B. A.; Bhattarai, A.; Mazur, U.; Hipps, K. W. Single molecule imaging of oxygenation of cobalt octaethylporphyrin at the solution/solid interface: Thermodynamics from microscopy. *J. Am. Chem. Soc.* **2012**, *134*, 14897–14904.
[130] Hulsken, B.; Van Hameren, R.; Gerritsen, J. W.; Khoury, T.; Thordarson, P.; Crossley, M. J.; Rowan, A. E.; Nolte, R. J. M.; Elemans, J. A. A. W.; Speller, S. Real-time single-molecule imaging of oxidation catalysis at a liquid-solid interface. *Nat. Nanotechnol.* **2007**, *2*, 285–289.
[131] Zhang, S. Y.; Liao, K.; Wang, J. J.; Chen, Z. Y.; Sun, B. W.; Wang, X.; Hu, W. B.; Han, X. P. Lewis acid-mediated interfacial accelerated mass transport and electron transfer for enhanced oxygen reduction electrocatalysis. *Nano Energy* **2025**, *146*, 111487.
[132] Ku, Y. P.; Kumar, K.; Hutzler, A.; Götz, C.; Vorochta, M.; Sougrati, M. T.; Lloret, V.; Ehelebe, K.; Mayrhofer, K. J. J.; Thiele, S. et al. Impact of carbon corrosion and denitrogenation on the deactivation of Fe–N–C catalysts in alkaline media. *ACS Catal.* **2024**, *14*, 8576–8591.
[133] Bai, P. Y.; Xu, L. Toward a unified pH-performance picture of active sites in nitrogen-doped carbon materials. *App. Catal. B: Environ. Energy* **2025**, *365*, 124908.